

Cross-Modality Neuroimage Synthesis: A Survey

GUOYANG XIE*, Southern University of Science and Technology, China and University of Surrey, United Kingdom

JINBAO WANG*, Southern University of Science and Technology, China

YAWEN HUANG*, Tencent Jarvis Lab, China

JIAYI LYU, University of Chinese Academy of Sciences, China

FENG ZHENG, Southern University of Science and Technology, China

YEFENG ZHENG, Tencent Jarvis Lab, China

YAOCHU JIN, Bielefeld University, Germany and University of Surrey, United Kingdom

Multi-modality imaging improves disease diagnosis and reveals distinct deviations in tissues with anatomical properties. The existence of completely aligned and paired multi-modality neuroimaging data has proved its effectiveness in brain research. However, collecting fully-aligned and paired data is expensive or even impractical, since it faces many difficulties, including high cost, long time duration, image corruption, and privacy issues. An alternative solution is to explore either unsupervised or weakly-supervised learning methods to synthesize the absent neuroimaging data. In this paper, we provide a comprehensive review of cross-modality synthesis for neuroimages, from the perspectives of weakly-supervised and unsupervised settings, loss functions, evaluation metrics, ranges of modality, datasets, and the synthesis-based downstream applications. We begin with highlighting several opening challenges for cross-modality neuroimage synthesis. Then, we discuss representative architectures of cross-modality synthesis methods under different supervisions. This is followed by a stepwise in-depth analysis to evaluate how cross-modality neuroimage synthesis improves the performances of its downstream tasks. Finally, we summarize the existing research findings and point out future research directions. All resources are available at <https://github.com/M-3LAB/awesome-multimodal-brain-image-synthesis>.

CCS Concepts: • **Applied computing** → **Health informatics**.

Additional Key Words and Phrases: cross-domain, multi-modality neuroimaging synthesis, medical image analysis, deep learning

ACM Reference Format:

Guoyang Xie, Jinbao Wang, Yawen Huang, Jiayi Lyu, Feng Zheng, Yefeng Zheng, and Yaochu Jin. 2018. Cross-Modality Neuroimage Synthesis: A Survey. In . ACM, New York, NY, USA, 25 pages. <https://doi.org/XXXXXXX.XXXXXXX>

1 INTRODUCTION

The necessity of cross-modality neuroimage synthesis. The majority of multi-center neuroimaging datasets [3, 78] are often high-dimensional and heterogeneous, which is shown in Fig. 1. For instance, positron emission tomography (PET) and magnetic resonance imaging (MRI) are the classic medical imaging techniques to provide detailed anatomic and physiologic images of different organs for auxiliary diagnosis or monitoring treatments. The paired/registered multi-modality data provide more complementary information to investigate certain pathology including neurodegeneration.

*The authors contributed equally to this research.

Permission to make digital or hard copies of all or part of this work for personal or classroom use is granted without fee provided that copies are not made or distributed for profit or commercial advantage and that copies bear this notice and the full citation on the first page. Copyrights for components of this work owned by others than ACM must be honored. Abstracting with credit is permitted. To copy otherwise, or republish, to post on servers or to redistribute to lists, requires prior specific permission and/or a fee. Request permissions from permissions@acm.org.

© 2018 Association for Computing Machinery.

Manuscript submitted to ACM

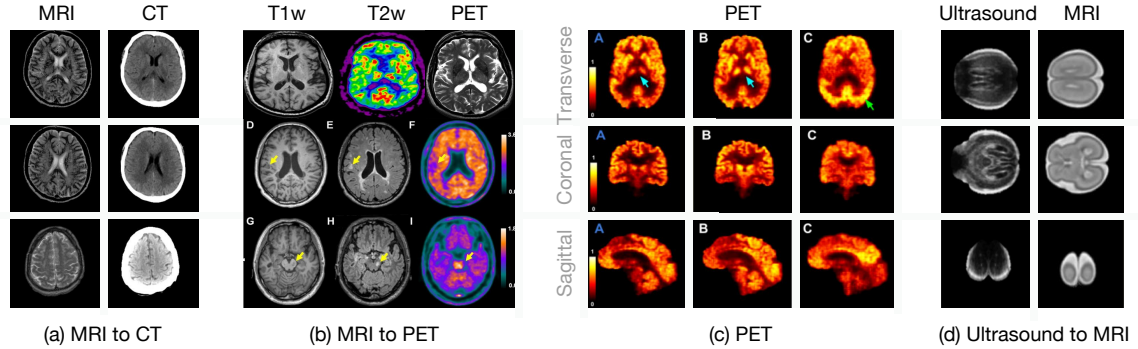


Fig. 1. Multi-modality synthesis. (a) MRI to CT [19], (b) MRI to PET [112], (c) PET [116], and (d) Ultrasound to MRI [41].

However, it is not feasible to acquire a full set of completely paired and aligned multi-modality neuroimaging data, considering that:

- Collecting multi-modality neuroimaging data is very costly. For example, a normal MRI can take more than one thousand dollars in some cities;
- Many medical institutions cannot share their data, since medical data are especially restricted by local regulations, despite that identifiable information can be removed for protecting the privacy of patients;
- Patients' motions may result in severe misaligned neuroimaging data.

As a result, there is a clear need to handle the absent data through a cross-modality synthesis method.

Cross-modality GAN in medical imaging community. Previously, the key problems in medical imaging community are: (1) how to fasten multi-contrast MRI reconstruction, (2) how to enhance the image quality of MRI or CT Scan, (3) medical image registration, and (4) fine-grained medical image segmentation. Experienced researchers can quickly iteratively construct innovative algorithms because the majority of them have rather mature answers, ensuring feasibility and high precision from design to product landing. Cross-modality neuroimage synthesis algorithms, however, are still in their infancy as of 2018 since the synthesis neuroimage quality cannot satisfy radiologist demands. The situation substantially changed when CycleGAN [118] emerges. We can easily observe that the number of the unsupervised learning methods and weakly-supervised learning methods is increasing from Fig. 2(a). The researchers have paid more attention to unsupervised learning and weakly-supervised learning methods. Fig. 2(b) indicates the number of various downstream tasks with each supervision level method. It can be easily observed that most of the unsupervised learning and weakly-supervised methods are jointly optimized with the segmentation task. But the classification and diagnosis tasks are ignored in unsupervised learning and weakly-supervised learning methods, to which we believe that future work should pay more attention. Fig. 2(c) presents modality synthesis according to the level of supervision. We notice that most of the algorithms conduct cross-modality synthesis for MRI. But PET and MRI to PET have not received enough attention in unsupervised learning and weakly-supervised learning algorithms. We expect future work should propose a uniform generator to synthesize an arbitrary modality among PET, MRI to PET, MRI to CT in a unsupervised learning or weakly-supervised learning manner.

Look back cross-modality neuroimage synthesis. From the standpoint of evolution, natural image-to-image translation lead the development of cross-modality neuroimage synthesis. Inspired by *dictionary learning* [1], Roy *et al.*

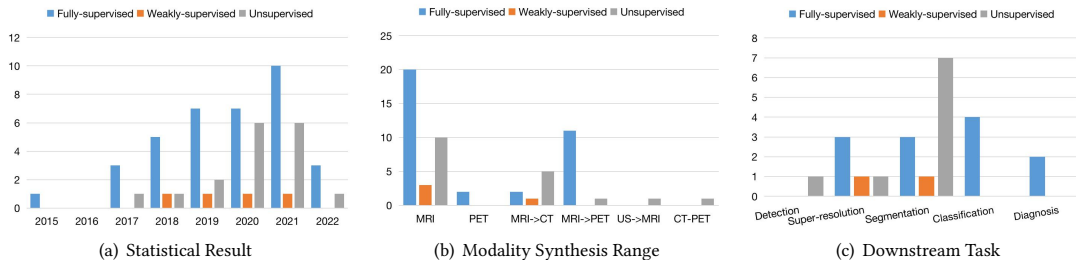


Fig. 2. Trend of each learning manner in multi-modality brain image synthesis. (a) the number of different levels of supervision papers published chronologically. (b) the number of the modality synthesis according to the level of supervision. (c) the number of various downstream tasks with each supervision level method.

al. [71] train two dictionaries where the input image is used to find the similar patches in a source modality dictionary and the corresponding target modality counterpart will be extracted in the target dictionary to generate the desirable modality data. The work of Huang *et al.* [30] improve the quality of cross-modality synthesis by imposing a graph Laplacian constraint in a joint dictionary learning framework. Wang *et al.* [85] synthesize the missing DT images from T1-w scans by learning a region enhanced joint dictionary. When *pix2pix* [39] is released in 2017, the situation drastically changes. Most of supervised cross-modality neuroimage synthesis algorithms adopt the variants of *pix2pix*. Maspero *et al.* [57] directly employ *pix2pix* to synthesize CT scans from MRI. The work of Olut *et al.* [64] synthesize magnetic resonance angiography (MRA) from T1 and T2 with the addition of steerable filter loss on *pix2pix*. Furthermore, *CycleGAN* [118] boost the performance of unsupervised cross-modality neuroimage synthesis. Hiasa *et al.* [25] employ a gradient consistency loss to optimize the edge map of synthesized neuroimage. Zhang *et al.* [113] propose two segmentation networks to segment the corresponding image modality into semantic labels and provides implicit shape constraints on the anatomy during translation. Chen *et al.* [9] propose a similar method with the work of Zhang *et al.* [113]. The only difference between them is that the segmentation network of Chen *et al.* [9] is trained offline and fixed during image translation network training phase. ***The inherent properties of medical image are ignored, despite the fact that natural image-to-image translation approaches reveal many insights to cross-modality neuroimage synthesis.*** For instance, Fig. 3 shows a fail case of *CycleGAN* [118] for cross-modality neuroimage synthesis. In particular, the lesion region of the target modality (red box of Fake A) cannot be accurately synthesized in comparison to the lesion region of the source modality (red dashed box of Real B), notably for the structural details. Hence, there is a need to deeply investigate to characterizing the network architecture for the imaging principle of brain image.

Comparison to other surveys. Table 1 shows the comparison for various survey in terms of levels of supervision, modality synthesis range and downstream task for synthesis. The work in [104] provides a comprehensive review of generative adversarial networks (GANs) in medical imaging before 2019, including single-modality synthesis, cross-modality synthesis and the usage of the GAN in different downstream tasks, e.g., classification, segmentation, registration. However, there are two constraints: (1) The work [104] was published in 2019, where most of the reviewed cross-modality synthesis methods [104] are supervised. In other words, most of synthesis algorithms require fully paired medical data for training. (2) The performance of the downstream tasks when leveraging the synthesized results are missing in the review, which we believe is of great importance, since the final purpose of cross-modality synthesis serves as an auxiliary procedure for the downstream tasks, e.g., segmentation. Another work in [114] comprehensively

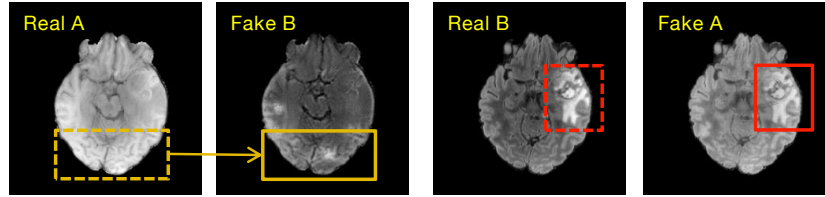


Fig. 3. A failed case in multi-modality brain image synthesis. In addition to generating low-resolution images, another problem is that the disease-related regions cannot be synthesized well. For example, when the target modality (Fake B) is generated from the input real modality (Real A), there exist failed regions (box) that are learned from the original ones (dashed box).

Table 1. Comparison on related surveys in terms of supervision level, modality synthesis range and synthesis for downstream tasks.

Survey	Supervision Level			Modality Synthesis Range					Synthesis for Downstream Tasks			
	Fully-	weakly-	Un-	MRI→MRI	PET→PET	MRI→CT	US→MRI	CT→PET	Segmentation	Classification	Registration	Diagnosis
Yi <i>et al.</i> [104]	✓			✓	✓	✓		✓				
Zhao <i>et al.</i> [114]	✓			✓					✓	✓	✓	✓
Ours	✓	✓	✓	✓	✓	✓	✓	✓	✓	✓	✓	✓

reviews the state-of-the-art deep learning-based methods applied in brain MRI, including segmentation, registration and diagnosis. It touches upon cross-modality brain synthesis but does not discuss this in detail. Furthermore, a taxonomy review is presented in [114], which focuses on the task without considering the level of supervision. In addition, it reviews brain MRI-related work, largely ignoring other common imaging ways like CT and PET.

Contributions. The main contributions of this survey paper can be summarized as follows:

- To the best of our knowledge, it is the first work to provide an in-depth review of cross-modality brain image synthesis by considering the level of supervision, especially for both unsupervised and weakly-supervised cross-modality synthesis.
- It provides a comprehensive review on the relationship between cross-modality synthesis and its downstream tasks. This survey focuses on how to make an appropriate cross-modality brain image synthesis to correctly improve the downstream tasks, such as image segmentation, registration and diagnosis.
- It summarizes the main issues and potential challenges in cross-modality brain image synthesis, which outlines the underlying research directions for future works.

Organization. The rest of the paper is organized as follows. We firstly introduce the chronological overview of cross-modality brain image synthesis and gives these methods in Section 2. In Section 3.1, we review cross-modality neuroimage synthesis on the basis of the level of supervision. Next, we review the recent advances in modality synthesis in Section 3.2. In Section 3.3, we provide an analysis of how cross-modality synthesis significantly improves the performance of the downstream task. Then, we describe the popular datasets in Section 4.1, review various loss functions in Section 4.2 and take a retrospective view of the metrics function in Section 4.3. In the end, we provide future research directions for brain neuroimage cross-modality synthesis in Section 5.

2 CHRONOLOGICAL REVIEW

Fig. 4 gives a chronological overview of the cross-modality brain synthesis methods according to the level of supervision, the relevant downstream tasks, and the range of modality synthesis. In 2013, Roy *et al.* [71] is the first

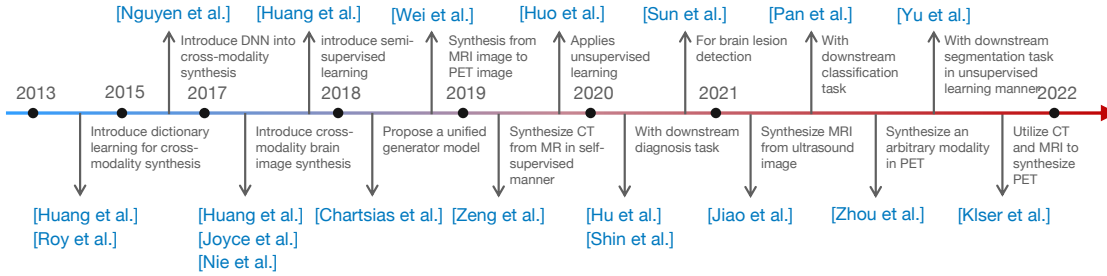


Fig. 4. A chronological review of multi-modality brain image synthesis.

one to introduce dictionary method [100] into cross-modality neuroimage synthesis. Ye *et al.* [103] propose a modality propagation method and prove that the proposed model can be derived from the generalization of label propagation strategy [22], and showed applications to arbitrary modality synthesis. In 2015, the work of Nguyen *et al.* [62] train a location-sensitive deep network to integrate intensity feature and spatial information, more accurately synthesizing the results to the same problem posed by [103]. In 2017, the works in [31, 43, 63] introduce the cross-modality brain image synthesis into the medical GAN community. Their methods are supervised, i.e., their training data are totally paired. Huang *et al.* [31] construct a closed loop filter learning strategy to learn the convolutional sparse coding (CSC), which is able to eliminate the requirement of large scale training data. Meanwhile, it is also the first one to undertake super-resolution and multi-modality neuroimaging data in MRI. The authors of [43] propose a multi-modality invariant latent embedding model for synthesis. The purpose of this method is to utilize the mutual information from multi-modality maximally and fuse them into the generated modality image. Nie *et al.* [63] introduce a synthesis method by translating brain MRI data to brain CT data. The authors incorporate the detailed information from brain MRI into GANs model to generate the brain CT data. After that, Huang *et al.* [32] provide a first weakly-supervised learning approach to cross-modality brain image synthesis. The work in [32] regards the unpaired data as an auxiliary resources. They propose a hetero-domain image alignment method to enforce the correspondence for unpaired auxiliary data, which can directly substantiate the benefits of the combination with a few paired data and massive unpaired data. Chartsias *et al.* [8] firstly propose a unified generator model for various MRI modalities. Huo *et al.* [37] firstly apply an unsupervised learning method to cross-modality brain image synthesis. In other words, the multi-modality training data are unpaired. Specifically, they adopt CycleGAN [118] to generate the target modality data from source modality data.

After that, the authors in [37] leverage both the synthesis modality data and the source modality data for segmentation. It is also the first one that has employed unsupervised learning methods for different downstream tasks. Wei *et al.* [92] provide a challenging synthesis approach to synthesize from MRI image to PET image. Specifically, Sketcher-Refiner GANs proposed by [92] decompose the synthesis problem as a sketch-refinement process, in which the sketchers generate the preliminary anatomical and physiological information, and the refiner refines the structure of tissue myelin content. Pan *et al.* [67] provide a method to jointly optimize both cross-modality synthesis task and the diagnosis task. They design a disease-image-specific network (DSNet) by feeding the features generated from disease-image-specific network into Feature-Consistency GANs (FC-GANs) to generate the target domain neuroimaging data. Since DSNet is closely associated with FC-GANs, the missing target domain data can be synthesized in a diagnosis-oriented manner. Hu *et al.* [28] and Shin *et al.* [76] are the first ones who have utilized the synthesized neuroimaging data to improve the

Table 2. A brief summary of cross-modality brain image synthesis methods used in the reviewed work (Part-I). Note that there are three levels of supervision (Sup.), i.e., fully supervised (F), weakly supervised (W) and unsupervised (U). The downstream task (DST) contains super-resolution (SR), segmentation (S), classification (C), detection (D), inpainting (I), registration (R), explainability (E), and diagnosis (Diag).

Publication	Name/Arch.	Sup.	Loss/Method	Dataset	Metrics	Align	DST
<i>MRI → MRI</i>							
Huang <i>et al.</i> [34]	WEENIE	W	Sparse coding	IXI, NAMIC	PSNR, SSIM	✓	SR
Huang <i>et al.</i> [31]	DOTE	F	Sparse coding	IXI, NAMIC	PSNR, SSIM	✓	SR
Huang <i>et al.</i> [29]	CoCa-GAN	F	$L_{gan}, L_{edge}, L_{gdl}, L_{tumor}$	BraTS15	PSNR, NMSE, SSIM	✓	
Huang <i>et al.</i> [35]	MCMT-GAN	F	$L_{gan}, L_{cyc}, L_{mani}, L_{fault}$	IXI, NAMIC	PSNR, SSIM, DSC	✓	S
Huang <i>et al.</i> [33]	WAG	W	$L_{spe}, L_{mmd}, L_{gcr}$	IXI, NAMIC	PSNR, SSIM	✓	
Huang <i>et al.</i> [36]	GAN	U	$L_{gan}, L_{cont}, L_{text}, L_{cyc}$	IXI, HCP	PSNR, SSIM	✗	SR, I
He <i>et al.</i> [20]	Autoencoder	U	L_{ae}, L_{oth}	IXI	MSE, SSIM	✗	
Yang <i>et al.</i> [99]	Hyper-GAN	U	$L_{gan}, L_{cyc}, L_{rec1}, L_{iden}, L_{cla}$	IXI, BraTS19	PSAR, SSIM, MAE	✗	
Sun <i>et al.</i> [80]	ANT-GAN	U	L_{gan}, L_{cyc}, L_{am}	BraTS18	P, R, F1S, VS	✗	S, D
Guo <i>et al.</i> [17]	CG-SAMR	U	$L_{gan}, L_{fm}, L_{sc}, L_{cm}, L_{rec1}, L_{cyc}$	D5	DSC	✗	S
Shen <i>et al.</i> [75]	REMIC	W	$L_{gan}, L_{cyc}, L_{rec1}, L_{dice}$	BraTS18, ProstateX	NRMSSE, PSNR, SSIM	✗	S, I
Tomar <i>et al.</i> [81]	SASAN	U	$L_{sgan}, L_{cyc}, L_{iden}, L_{reg}, L_{dice}$	BraTS15	DSC, ASSD	✗	S
Charsias <i>et al.</i> [8]	Autoencoder	F	L_{ae}	ISLES15, BraTS15, IXI	MSE, PSNR, SSIM	✓	
Chen <i>et al.</i> [11]	ABCNet	F	$L_{gan}, L_{sm}, L_{tiu}, L_{cor}$	BCP, dHCP, HCP	DSC, ASSD, CC, CIV, HD95	✓	
Bne <i>et al.</i> [6]	Autoencoder	F	L_{rec2}	–	PSNR, SSIM, L2, t-L2	✓	
Dar <i>et al.</i> [13]	pGAN	F	$L_{cgan}, L_{p2p}, L_{prec}, L_{cyc}$	MIDAS, IXI, BraTS15	PSNR, SSIM	✗	
Jog <i>et al.</i> [42]	REPLICA	F	Random forest	MMRR	PSNR, SSIM, UQI	✓	
Joyce <i>et al.</i> [43]	Autoencoder	F	L_{p2p}	ISLES15, BraTS15	MSE	✗	
Kwon <i>et al.</i> [47]	Autoencoder	F	L_{gan}	ANDI, BraTS18, ATLAS	MMD, MSSSIM	✓	
Qu <i>et al.</i> [70]	MCGAN	U	$L_{gan}, L_{ssim}, L_{rec2}, L_{cyc}, L_{edge}$	BraTS15	PSNR, SSIM, DSC	✓	S
Lee <i>et al.</i> [49]	CollaGAN	F	L_{gan}, L_{ssim}	D9	NMSE, SSIM	✓	
Li <i>et al.</i> [50]	DiamondGAN	F	L_{rec1}, L_{gan}	D10	PSNR, MAE	✗	
Liu <i>et al.</i> [53]	Conditional GAN	F	L_{gan}, L_{p2p}, L_{mc}	BraTS18	L1, SSIM, PSNR, IS	✓	S
Sharma <i>et al.</i> [74]	MM-GAN	F	L_{sgan}, L_{p2p}	ISLES15, BraTS18	MSE, PSNR, SSIM	✓	
Xin <i>et al.</i> [97]	TC-MGAN	F	$L_{gan}, L_{p2p}, L_{cls}, L_{seg1}$	BraTS18	PSNR, SSIM	✓	
Yang <i>et al.</i> [101] [102]	cGANs	U	L_{cgan}, L_{rec1}	MRBrainS13, ANDI, RIRE, iSeg17, BraTS15	MAE, PSNR, MI, F-score, DSC	✓	S, R
Yu <i>et al.</i> [106]	SA-GAN	F	L_{gan}, L_{iden}	BraTS15, SSIS15	PSNR, NMSE, SSIM	✓	
Yu <i>et al.</i> [105]	3D cGAN	F	L_{cgan}, L_{iden}	BraTS15	PSNR, NMSE, DSC	✓	S
Yurt <i>et al.</i> [108]	mustGAN	F	L_{cgan}, L_{iden}	IXI, ISLES15	PSNR, SSIM	✓	
Zhou <i>et al.</i> [117]	Hi-Net	F	L_{cgan}, L_{rec1}	BraTS18, ISLES15	PSNR, SSIM, NMSE	✓	
Zuo <i>et al.</i> [119]	DMC-Fusion	F	L_{rec1}, L_{ssim}	D15	MI, Q, FMI, PSNR, SSIM	✓	
Bian <i>et al.</i> [5]	DDA-Net	U	$L_{gan}, L_{cyc}, L_{seg}$	MRBrainS18	DSC, SEN, SPE, ROC	✓	S
<i>MRI → CT</i>							
Hemsley <i>et al.</i> [23]	cGAN	W	L_{cgan}, L_{p2p}	D1	MAE	✓	
Huo <i>et al.</i> [37]	SynSeg-Net	U	$L_{gan}, L_{cyc}, L_{seg}$	D3	DSC, ASD	✗	S
Yang <i>et al.</i> [98]	sc-cycleGAN	U	L_{sgan}, L_{cyc}	D6	MAE, PSNR, SSIM	✗	
Zeng <i>et al.</i> [110]	2D-cGAN	U	$L_{sgan}, L_{cyc}, L_{rec1}$	D7	MAE, PSNR	✗	
Klser <i>et al.</i> [45]	pCT	U	L_{rec2}	D8	MAE	✓	
Nie <i>et al.</i> [63]	GAN	U	L_{gan}, L_{gdl}	ANDI	PSNR, MAE	✓	
Zuo <i>et al.</i> [119]	DMC-Fusion	F	L_{rec1}, L_{ssim}	D15	MI, Q, FMI, PSNR, SSIM	✓	
Huynh <i>et al.</i> [38]		F	Random forest	ANDI	MAE, PSNR	✓	

performance of a classification task. Zhou *et al.* [116] propose a generator to synthesize an arbitrary modality in PET. Klser *et al.* [45] utilize two modalities data, i.e., CT and MRI, to synthesize PET data. Yu *et al.* [107] jointly optimize the synthesis and segmentation problems by using the unsupervised learning methods. Jiao *et al.* [41] synthesize MRI from ultrasound image using a new fusion scheme to utilize various modality from unpaired data. Zeng *et al.* [110] synthesize CT from MR by using the self-supervised methods.

3 METHODS

Table 2 and Table 3 offer an taxonomy for the work covered in this survey. Specifically, the second column in the tables is the proposed architecture name. The third column denotes the level of supervision, i.e., fully-supervised (F), weakly-supervised (W), or unsupervised (U) manner. The fourth through sixth columns, respectively, indicate the loss

Table 3. A brief summary of cross-modality brain image synthesis methods used in the reviewed publications (Part-II). Note that there are three levels of supervision (Sup.), i.e., fully supervised (F), weakly supervised (W) and unsupervised (U) manner. Downstream task (DST) contains super-resolution (SR), segmentation (S), classification (C), detection (D), inpainting (I), registration (R), explainability (E), and diagnosis (Diag).

Publication	Name/Arch.	Sup.	Loss/Method	Dataset	Metrics	Align	DST
<i>MRI → PET</i>							
Wang <i>et al.</i> [88]	LA-GANs	F	L_{egan}, L_{p2p}	D2	PSNR	✓	SR
Hu <i>et al.</i> [28]	Bidirectional GAN	F	$L_{gan}, L_{rec1}, L_{prec}, L_{kl}$	ADNI	PSNR, SSIM	✓	
Hu <i>et al.</i> [27]	BMGAN	F	$L_{gan}, L_{rec1}, L_{prec}, L_{kl}$	ADNI	MAE, PSNR, MSSSIM, FID	✓	
Liu <i>et al.</i> [54]	JSRL	F	$L_{gan}, L_{rec1}, L_{cls}$	CLAS, ADNI, AIBL	AUC, BAC, SEN, SPE, F1S	✓	C
Pan <i>et al.</i> [66]	LM ³ IL	F	L_{gan}, L_{cyc}	ADNI	ACC, SEN, SPE, F1S, MCC, AUC	✓	C
Pan <i>et al.</i> [65] [68]	FGAN	F	L_{gan}	ADNI	MAE, SSIM, PSNR, AUC, ACC, SPE, SEN, F1S, MCC	✓	C
Shin <i>et al.</i> [76]	GANDALF	F	$L_{egan}, L_{p2p}, L_{cls}$	ADNI	ACC, P, R	✓	C
Wei <i>et al.</i> [92]	Sketcher-Refiner GAN	F	L_{egan}, L_{rec1}	D13	DVR	✓	
Zuo <i>et al.</i> [119]	DMC-Fusion	F	L_{rec1}, L_{ssim}	D15	MI, Q, FMI, PSNR, SSIM	✓	
Kao <i>et al.</i> [44]	ESIT	U	L_{rec1}	ANDI	MAE, PSNR, SSIM	✓	E
Zhang <i>et al.</i> [111]	BPGAN	F	$L_{gan}, L_{rec1}, L_{kl}$	ANDI	MAE, PSNR, SSIM	✓	Diag
<i>CT → PET</i>							
Klser <i>et al.</i> [45]	pPET	F	L_{rec2}	D8	MAE	✓	
<i>US → MRI</i>							
Jiao <i>et al.</i> [41]	GAN	U	L_{gan}, L_{p2p}	D4	MOS, DS	✗	
<i>PET → PET</i>							
Wang <i>et al.</i> [89]	LA-GANs	F	L_{gan}, L_{rec1}	D11, D12	PSNR, SSIM	✓	SR
Zhou <i>et al.</i> [116]	UCAN	F	$L_{gan}, L_{iden}, L_{cls}, L_{cyc}$	D14	NMSE, SSIM	✓	Diag

function, the metrics employed, and whether the input neuroimage images are aligned or misaligned. The last column refers the downstream task (DST), which contains super-resolution (SR), segmentation (S), classification (C), detection (D), inpainting (I), registration (R), explainability (E), and diagnosis (Diag). We will discuss each of them in the following sections.

3.1 Learning Paradigms

3.1.1 Fully-Supervised Methods. For dictionary learning based method, before 2018, most of synthesis algorithms adopt CSC filter [109]. But the major drawback of CSC is that it requires a huge amount of paired data in training. The work in [31, 32] employ a dual filter training strategy and hetero-domain image alignment to significantly reduce the requirement of a huge amount of paired data. When pix2pix was released in 2017, an alternative generative model, GAN, become the mainstream for cross-modality neuroimaging data synthesis [77, 88]. Zhou *et al.* [117] pay more attention to the layer-wised fusion strategy from multiple input modality data and designs a Mixed Fusion Block (MFB) to combine the latent representation from each source modality. Kwon *et al.* [47] apply the alpha-GAN to generate 3D brain MRI from a random vector. Huang *et al.* [29] project multi-modality brain MRI data into one common feature space and utilize the modality invariant information represented in the common feature space to generate the missing target domain image space. After that, they apply gradient-weighted class activate mapping (GradCAM) [73] to interpret why the synthesis neuroimaging could be utilized for potential clinical usage. Yurt *et al.* [108] utilize multi-modalities neuroimaging data and fuse their features to generate the target domain data. Jog *et al.* [42] adopt a multi-scale feature extraction scheme and feed the features to three random forest trees to predict the corresponding area of target modality data. CollaGAN is proposed by [49], which utilizes the invariant embedding features from multi-modality data and fuses their information to synthesize the target modality data. However, supervised cross-modality neuroimage synthesis algorithms are challenging for product launch because they need a high number of neuroimage data pairs for training, which is difficult to get at medical institutions owing to patients' privacy concerns.

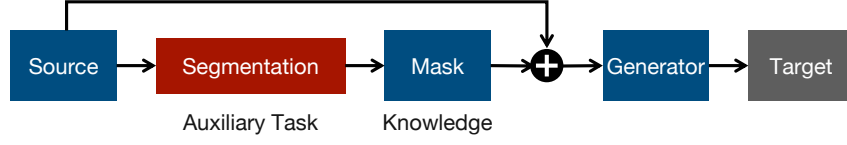


Fig. 5. Weakly-supervised architecture with an auxiliary task.

3.1.2 Weakly-Supervised Methods. We category weakly-supervised cross-modality neuroimage synthesis algorithm into two steams. As illustrated in Fig. 5, the first stream is to utilize a cross-modality segmentation mask to extract the knowledge from the lesion region [75]. Then, the knowledge from the segmentation mask is distilled to the generator. In other words, the segmentation network was treated as a teacher to guide the generator by using unpaired training data. We think that this method is a potential solution to solve the problem that described in Fig. 3. Since this method transfer the knowledge from the lesion region to the generator, it is possible to make the generator to pay more attention to the lesion region and synthesize a high-fidelity neuroimage. The second stream [33, 34] aims to make use of a few paired neuroimage dataset at first and extract the feature from each modality. After that, Huang *et al.* [33] project each modality's feature points into the common feature space and adopt maximum mean discrepancy (MMD) to calculate the divergence of paired feature points in the reproducing common feature space. In the end, the new feature from the incoming unpaired source modality neuroimage data employs MMD to seek the intrinsic pair feature points in the common feature space. The new target modality neuroimage is generated by feeding the pair feature points from the common feature space into the generator. The flowchart of the second stream method is given in Fig. 6.

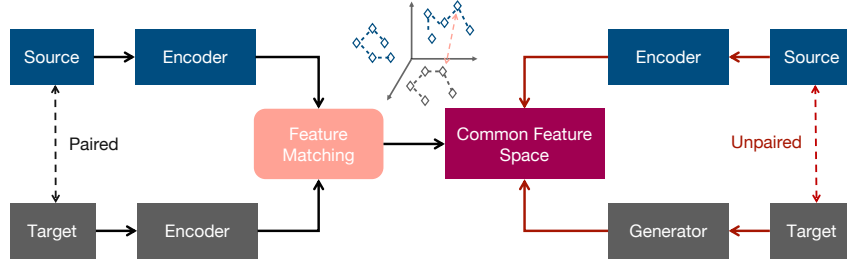


Fig. 6. Weakly-supervised architecture via projecting into the common feature space.

3.1.3 Unsupervised Methods. The main stream for unsupervised cross-modality neuroimage synthesis is CycleGAN [118]. In Fig. 7, CycleGAN is separated into two loops. The first loop is source domain \rightarrow synthesis target domain \rightarrow reconstructed source domain. The second loop is target domain \rightarrow synthesis source domain \rightarrow reconstructed target domain. CycleGAN [118] utilize two loops to construct a cycle loss function, which is described as below:

$$\mathcal{L}_{cycle} = \mathbb{E}_{\mathbf{X} \sim p_r(\mathbf{X})} \|\mathbf{X} - F(G(\mathbf{X}))\|_1 + \mathbb{E}_{\mathbf{Y} \sim p_r(\mathbf{Y})} \|\mathbf{Y} - G(F(\mathbf{Y}))\|_1, \quad (1)$$

where X denotes the source domain and Y denotes the target domain. G and F are the generators for task $X \rightarrow Y$ and task $Y \rightarrow Y$. The GAN loss function in CycleGAN [118] is described as below:

$$\begin{aligned} \mathcal{L}_{adv} = & \mathbb{E}_{\mathbf{Y} \sim p_r(\mathbf{Y})} [\log D_G(\mathbf{Y})] + \mathbb{E}_{\mathbf{X} \sim p_r(\mathbf{X})} [\log (1 - D_G(G(\mathbf{X})))] \\ & + \mathbb{E}_{\mathbf{X} \sim p_r(\mathbf{X})} [\log D_F(\mathbf{X})] + \mathbb{E}_{\mathbf{Y} \sim p_r(\mathbf{Y})} [\log (1 - D_F(F(\mathbf{Y})))] . \end{aligned} \quad (2)$$

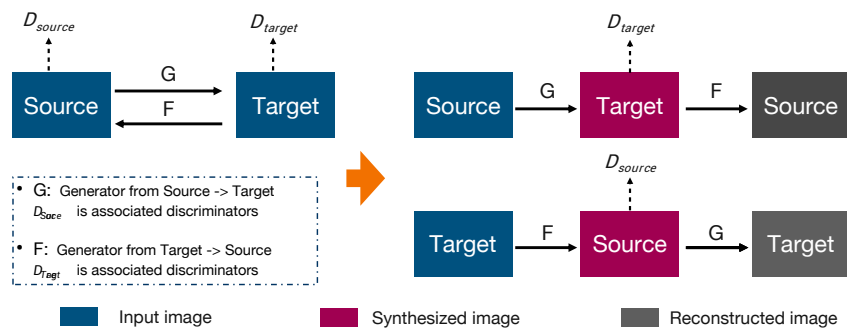


Fig. 7. CycleGAN [118] architecture.

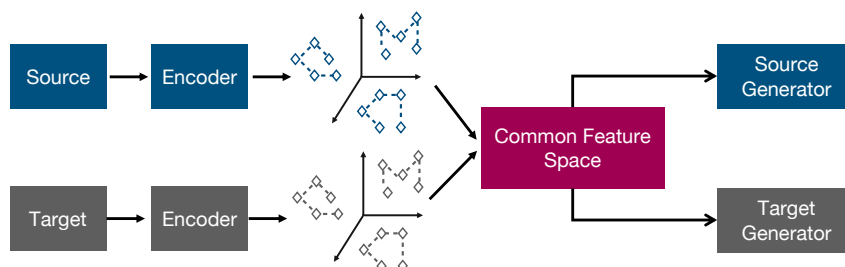


Fig. 8. Unsupervised learning architecture [35] for cross-modality neuroimage synthesis.

Most variants of unsupervised cross-modality synthesis are built on the base of the cycle loss in Equation 1 and the adversarial loss in Equation 2. Among them, the main difference usually lies in the feature extraction and alignment [35, 41, 110]. The work presented in Huang *et al.* [35] is one of classical models.

In Fig. 8, the unpaired source modality and the target modality neuroimages are fed into the modality specific feature encoder. The authors in [35] utilize extended multi-kernel maximum distance to calculate the distance of features from different modalities. If the distance of features is closer than certain threshold value, MCMTGAN [35] aligns them as the paired feature points and constructs a common feature space. In the inference phase, the new unpaired source modality is fed into the modality specific feature encoder to obtain the reference feature point. Then MCMTGAN seek the paired feature points from the common feature space. The seek feature paired points are fed into the modality-specific generators to synthesize cross-modality neuroimages. Yu *et al.* [107] provide a similar work with the method shown in [35]. However, the authors pay more attention to the mouse brain dataset. Chen *et al.* [10] propose a more concise idea, i.e., the source modality and the target modality share their feature encoder. Jiao *et al.* [41] also extract the feature and map them into the common space from different modalities. Moreover, the author in [41] design a new cross-modal attention module for fusion and propagation. Zeng *et al.* [110] use two models, one of which is the 3D generator network and the other is the 2D discriminator. The authors utilize the result from the 2D discriminator treated as a weak label to supervise the 3D generator, such that the output of the generator can be closer to the output of CT. Yang *et al.* [99] design a uniformed generator for MRI synthesis. The method is also similar to [35], which mainly depends on the common feature space. Yang *et al.* [98] also borrow the concept of the common feature space and design a module to make the features from various modalities closer. Tomar *et al.* [81] develop a learnable self-attentive spatial

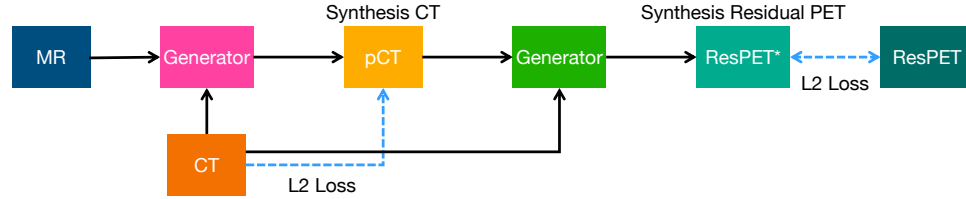


Fig. 9. MRI to CT and PET architecture [45].

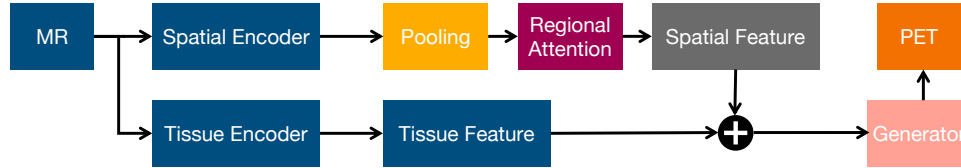


Fig. 10. MRI to PET architecture [44].

normalization with a GAN, which can greatly improve the generator’s performance. He *et al.* [20] treat the synthesis problem as the domain generalization problem. The performance of the generator on the unseen target modality cannot be guaranteed due to the domain shift problems.

3.2 Modality Synthesis Range

3.2.1 MRI To CT. Computed tomography (CT) is of great importance for different clinical applications, such as PET attenuation correction and radiotherapy treatment planning. However, the patients need to be exposed in radiation during CT acquisition, which may cause side-effects. But MRI is much safer than CT. There is a clear need to synthesize CT [37, 63, 110] from MRI. In Fig. 1(a), the first column denotes MRI and the second column denotes its paired CT. One of classical architecture [45] is shown in Fig 9. Klsler *et al.* [45] construct two networks. The role of the first network is to generate CT (pseudo CT) from MRI. The role of the second network is to generate PET from pseudo CT. The total training process can be divided into two parts. The first part is to make pseudo CT more consistent with the real CT, and the second part aims to make the generated PET more consistent with the real PET. In the first part of training stage, the authors feed the paired MR and CT into the first generator. The synthesized CT and the input CT construct a L2 loss function to optimize the parameters of the first generators. In the second part of training stage, the authors feed the synthesized CT and the real CT into the second generator. The synthesized residual PET and the ground truth residual PET formulate a L2 loss function to optimize the parameters of the second generator.

3.2.2 MRI To PET. Positron emission tomography (PET) is a very essential measure to measure myelin content changes in-vivo in multiple sclerosis. However, PET imaging is very expensive and invasive due to the injection of a radioactive tracer. In contrast, MRI is much safer since it is not invasive. Therefore, it significantly motivates the researchers to synthesize MRI from PET [92]. In addition, PET is also regarded as the gold standard for the diagnosis of Alzheimer’s disease (AD). As previous mentioned, PET can be prohibitive due to the cost and invasive nature. Shin *et al.* [76] propose an conditional GAN to synthesis from MRI to PET, where the auxiliary information is from AD diagnosis. Liu *et al.* [54] employ a GAN to synthesize PET from MRI and then feed the generated PET and real MRI into the segmentation task.

Hu *et al.* [27] employ a bidirectional mapping mechanism to synthesize MR to CT and CT to MR simultaneously. Kao *et al.* [44] propose to lay the explanatory groundwork for the cross-modal medical image translation model by exploring the biological plausibility behind the deep neural net, particularly focusing on the T1-MRI to PET translation, as shown in Fig. 1(b). The architecture details are shown in Fig. 10. The input MRI is fed into two feature encoder. One is the spatial encoder, the other is tissue encoder. The spatial feature and the tissue feature are merged and sent into the generator to synthesize the target PET.

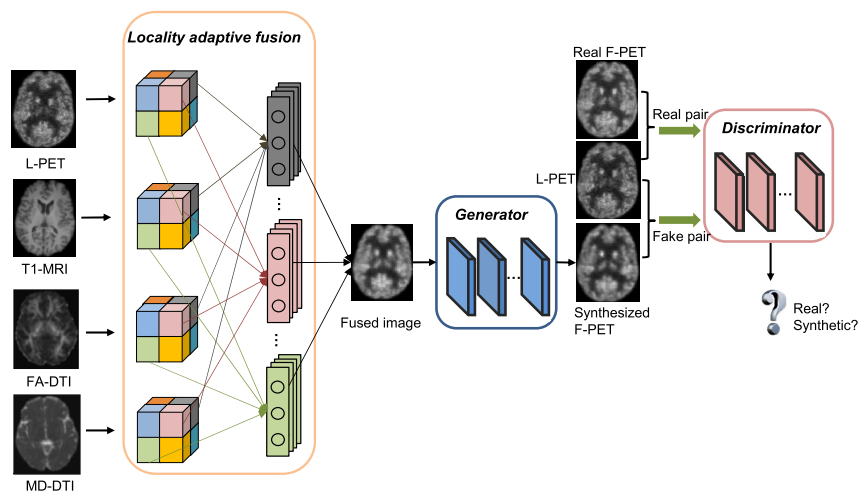


Fig. 11. PET synthesis architecture [89].

3.2.3 PET. Unlike previous methods, i.e., one-to-one fixed modality translation, Zhou *et al.* [116] propose a 3D unified cycle-gan (UCAN) to synthesize the arbitrary modality in PET, as shown in Fig. 1(c). Another method is proposed by Wang *et al.* [89], which is shown in Fig. 11. They propose a 3D auto-encoder to capture various PET modality features into one common space and then utilize the common feature space for synthesize arbitrary PET modalities. In specific, the input data contains PET, MRI and DTI modalities neuroimages. The shared feature encoder extracts the feature from modality-specific neuroimage. Then the feature map from different modalities are aligned to generate the fused image via the proposed locality adaptive fusion block. The fused image are fed into the generator to synthesis different modalities-paired neuroimages. The role of the discriminator is to classify whether these synthesized paired neuroimages are real or fake.

3.2.4 Ultrasound to MRI. Ultrasound (US) is the most common method to detect abnormalities in the fetal brain and growth restriction. However, the quality of ultrasound is easily affected by acoustic windows and occlusions, which mainly come from fetal brain skull. MRI is unaffected by this case and is able to provide more complete spatial details for full anatomy. One major drawback is that the paired data for ultrasound and MRI is extremely difficult to collect. Jiao *et al.* [41] employ the self-supervised methods to synthesize MRI from ultrasound images, as shown in Fig. 1(d). In Fig. 12, the ultrasound neuroimage and the MRI neuroimage are fed into the modality-specific feature encoder. And all features are aligned in one common feature space. The appearance and the edge feature of MRI and Ultrasound are used to constrain the reconstruction process.

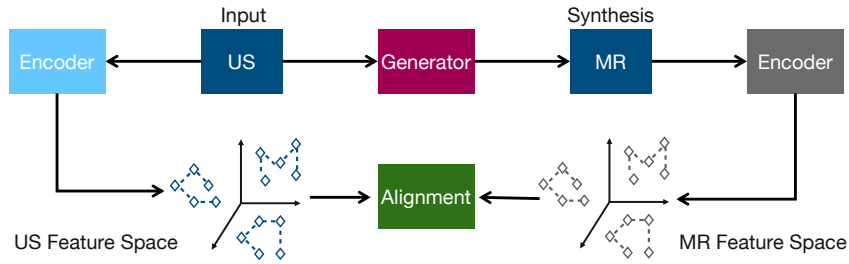


Fig. 12. Ultrasound (US) to MRI overall architecture [41].

3.3 Downstream Tasks

3.3.1 Segmentation. We summarize how the segmentation task is incorporated into cross-modality neuroimage synthesis. In general, there are two methods. The aim of the first method is to utilize cross-modality synthesis neuroimage to improve the performance of segmentation mask. The architecture detail is shown in Fig. 13. The synthesis target modality neuroimage and the input modality neuroimage are concatenated and fed into the the segmentation mask [37, 75, 107]. Huo *et al.* [37] directly use the accuracy of the segmented results to evaluate whether the synthesized data is helpful, without evaluating the quality of the synthesized results by PSNR and SSIM. Yu *et al.* [107] jointly optimize the synthesis task and the segmentation task by using an unsupervised learning method. Furthermore, The aim of the second method is to utilize a segmentation mask to boost the performance of cross-modality neuroimage synthesis [11, 17, 115].

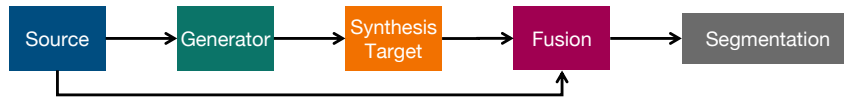


Fig. 13. Segmentation architecture of first method [75].

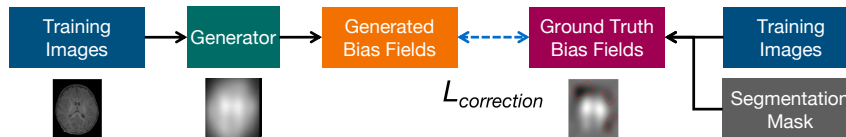


Fig. 14. Segmentation architecture of second method [11].

For instance, the architecture of Chen *et al.* [11] is shown in Fig. 14. To be specific, the training images and the segmentation mask generate the ground truth bias fields via N4. Then the synthesis bias fields and the ground truth bias fields formulate a correction loss to optimize the parameters of generators. Chen *et al.* [11] pay more attention to the brain MRI of infant. The authors [11] incorporate the manual annotations of tissue segmentation maps into the synthesis procedure and make the generated data to be more segmented-oriented. Finally, the work in [11] proves that the synthesized maps can significantly improve the segmentation accuracy. Guo *et al.* [17], Shen *et al.* [75] and Zhou *et al.* [115] leverage the segmentation task to guide the synthesis task.

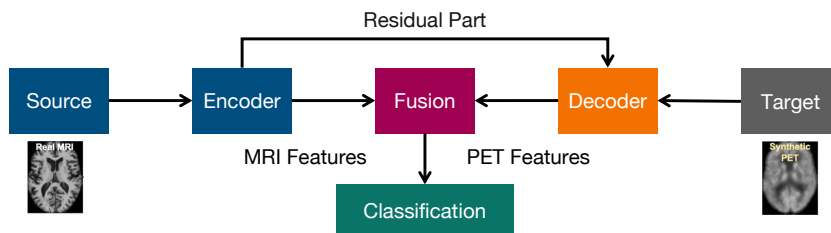


Fig. 15. Classification architecture [54].

3.3.2 Classification. In Fig. 15, we summarize how the classification task is incorporated into cross-modality neuroimage synthesis. The feature embedding from the input source modality neuroimage and the feature embedding from the synthesis target modality are mixed as the input for the classification task [28, 54, 76]. Similar to Fig. 15, the work in [76] incorporate AD’s information as the auxiliary method to improve the performance of target modality image synthesis. Since the synthesis process is classification-oriented, the synthesized brain image can largely improve the performance of AD’s classification. Hu *et al.* [28] design a bidirectional mapping mechanism to preserve the brain structures into the high-dimensional details. The work in [28] verifies that the synthesized neuroimaging data can improve the classification accuracy.

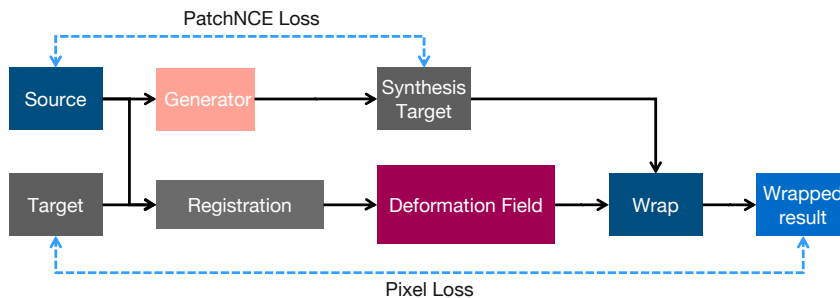


Fig. 16. Registration architecture [12].

3.3.3 Registration. Multi-modality neuroimage registration [55] is a traditional topic for medical image community. But utilizing cross-modality neuroimage synthesis for registration [12, 21] is the upcoming trend. One representative example is given in [12]. Its architecture detail is shown in Fig. 16. The model consists of two components. One is the registration network and the other is cross-modality synthesis network. Both of them are jointly optimized. The source modality neuroimage is warped to align with the target image via the deformation field. Then the authors in [12] propose a novel PatchNCE loss to preserve the shape information for the synthesis neuroimage. Furthermore, Chen *et al.* [12] employs a pixel-wise reconstruction loss function to preserve the appearance of the synthesis neuroimage. In this case, the proposed model is able to optimize the generator and registration network simultaneously.

3.3.4 Diagnosis. Pan *et al.* [67] is the first work to apply cross modality neuroimage synthesis to diagnosis tasks. The training stage is divided into three stages. The whole architecture details are described in Fig. 17. In the first stage, the input source modality neuroimage and its paired target modality neuroimage are fed into the feature encoder to

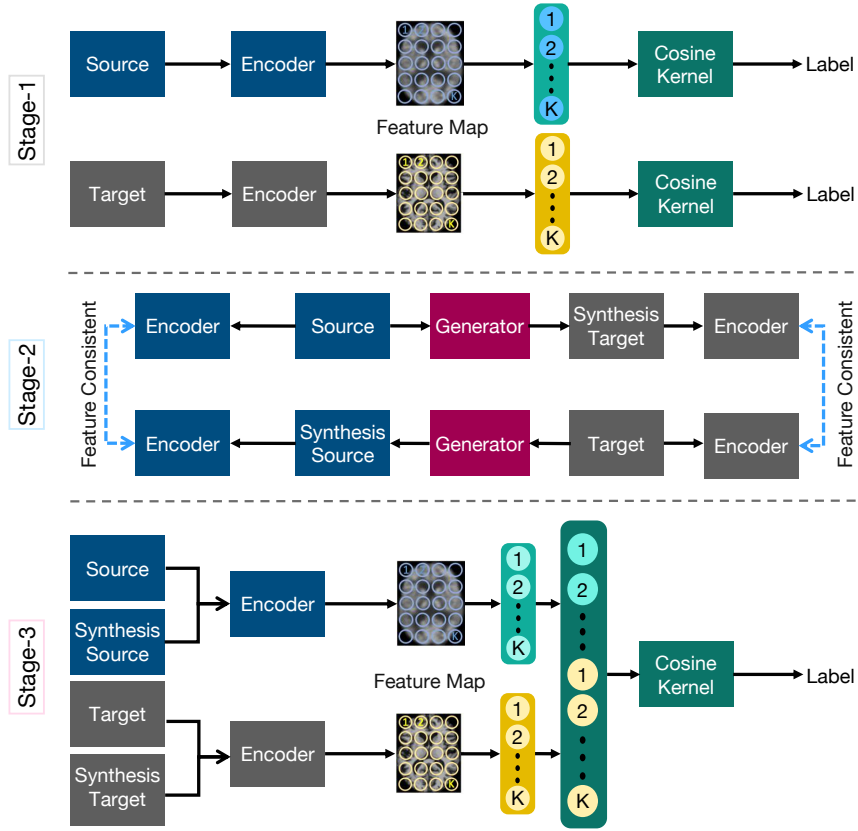


Fig. 17. Diagnosis architecture [67].

obtain the modality-specific feature map. Pan *et al.* [67] propose a spatial cosine kernel function to decompose the output feature map into two part. One is the disease-relevant part and the other is the residual normal part, which is not relevant to the disease. The purpose of spatial cosine kernel is to make sure that the classifier can learn the disease-relevant features. In the second stage, the source feature encoder and the target feature encoder are frozen. In other words, only the generator is trained with end-to-end manner. The aim of the second stage is to encourage the feature map from the synthesis neuroimage is consistent with the feature map from the input neuroimage. In the third stage, the feature from the source modality neuroimage and the target modality neuroimage are concatenated for the brain disease identification. Pan *et al.* [67] utilize the synthesized neuroimaging data for assisting disease diagnosis. However, this work adopts a supervised learning method by inputting paired multi-modality neuroimaging data, which is difficult to be applied to other tasks, since it is very difficult to collect fully paired data.

4 DATASET, LOSSES AND METRICS

4.1 Datasets

A summary of the public datasets is presented in Table 4. It can be easily observed that most of public datasets can only be conducted on MRI-to-MRI synthesis. There is no dataset for MRI to PET, MRI to CT or CT to PET synthesis.

Table 4. A brief summary of datasets reviewed in this work. The first column denotes the name of public dataset. The second column denotes the modality synthesis. The third column is data description, including the data size, data collection site, data collection machinery, and the purpose of data usage. Note that # and † indicate that it has labels for the segmentation task and classification task, respectively.

Dataset	Subjects	Modality	Data Description
<i>Public</i>			
IXI	578	MR (T1w, T2w, PDw)	Healthy subjects, 3 hospitals with different mechanisms, $256 \times 256 \times z$ ($z = 112 - 136$). URL: http://brain-development.org/ixi-dataset .
BRATS15 [60]	65 [#]	MR (T1, T1c, T2, FLAIR)	Multi-contrast MR scans from glioma patients. URL: https://www.smir.ch/BRATS/Start2015 .
BRATS18 [7]	285 [#]	MR (T1w, T2w, FLAIR)	210 high grade glioma (HGG) and 75 lower grade glioma (LGG) MRI with binary masks for the tumor (or lack of tumor). Each 3D MRI contains 155 slices of size 240×240 . URL: https://www.med.upenn.edu/sbia/brats2018.html .
BRATS21	2000 [#]	MR (T1, T2, FLAIR)	URL: http://www.brain-tumor-segmentation.org .
NAMIC	20	MR (T1w, T2w)	10 normal controls and 10 schizophrenic, $128 \times 128 \times z$ ($z = 88$). URL: https://www.na-mic.org/wiki/Downloads .
HCP [84]	200	MR (T1w, T2w)	The human connectome project (HCP), but for healthy young-adult subjects. URL: https://www.humanconnectome.org .
BCP [26]	546	MR (T1w, T2w)	Real infant MRI scans.
ProstateX [52]	98	MR (T2w, ADC, DWI)	Contain 3 modalities: T2w, apparent diffusion coefficient (ADC), high b-value DWI images.
ISLES15 [56]	65 [#]	MR (T1w, T2w, FLAIR, DWI)	Ischemic stroke lesion segmentation (ISLES), a medical image segmentation challenge at the International Conference on MICCAI 2015. URL: http://www.isles-challenge.org/ISLES2015
MIDAS [13]	66	MR (T1w, T2w)	48 subjects for training, 5 for validation and 13 for testing.
ANDI [40]	680 [†]	MR (T1w), PET	Alzheimer disease neuroimaging initiative (ADNI). URL: https://adni.loni.usc.edu .
MMRR [48]	21	MR (T2w)	Multimodal reproducibility resource (MMRR).
ATLAS [51]	220	MR (T1w)	Anatomical tracings of lesions after stroke (ATLAS), for stroke MRI generation. URL: http://fcon_1000.projects.nitrc.org/indi/retro/atlas.html .
CLAS	76	MR (T1w)	Chinese longitudinal aging study (CLAS).
AIBL [14]	235	MR (T1w), PET	Australian imaging, biomarkers and lifestyle (AIBL), paired T1w MRI and Flute/PIB-PET scans.
MRBrainS13 [59]	20 [#]	MR (T1, FLAIR)	URL: https://mrbrains13.isi.uu.nl .
MRBrainS18	7 [#]	MR (T1, FLAIR)	Providing ground truth labels for 10 categories of brain structures. URL: https://mrbrains18.isi.uu.nl .
iSeg17 [87]	23 [#]	MR (T1, T2)	661 training images, 163 images for testing.
RIRE [93]	19	MR (T1, T2)	Including T1 and T2 images collected from 19 subjects.
<i>Private</i>			
D1 [23]	105	MR (T1w, FLAIR), CT	matrix size 512×512 .
D2 [88]	16	MR (T1), PET	8 normal control subjects and 8 mild cognitive impairment subjects, each with an low-dose PET image, a T1-MRI image and an full-dose PET image. Each aligned image has the resolution of $2.09 \times 2.09 \times 2.03 \text{ mm}^3$ and the image size of $128 \times 128 \times 128$.
D3 [37]	60MRI, 19CT	MR (T2w), CT	In total, 3262 MRI slices and 1874 CT slices were used in the experiments.
D4 [41]	107US, 2MRI	MR, US	Around 36,000 2D US slices and 600 MRI slices were extracted accordingly.
D5 [17]	100	MR (T1w, T2w, FLAIR)	$256 \times 255 \times 15$, 3 labels: edema; cavity; and tumor.
D6 [98]	45	MR, CT	Training set of 28 subjects, validation set of 2 subjects, and test set of 15 subjects.
D7 [110]	50	MR, CT	2 modalities are aligned with a rigid registration, $256 \times 288 \times 112$.
D8 [45]	20MRI, 18PET	MR (T1w, T2w), PET	20 pairs of brain MR, CT and 18F-FDG PET images.
D9 [49]	10	MR (T1F, T2w, T2F)	Total 280 axis brain images were scanned and the additional T2 FLAIR sequence from 10 subjects. There are four types of MR contrast images in the dataset: T1-FLAIR, T2w, T2-FLAIR, and T2-FLAIR*.
D10 [50]	65	MR (T1, T2, FLAIR, DIR)	65 scans of patients with MS lesions from a local hospital.
D11 [89]	20	MR (T1), PET	20 simulated subjects were generated from the BrainWeb database of twenty normal brains.
D12 [89]	16	MR (T1), PET	8 normal control subjects and 8 mild cognitive impairment subjects, each with an L-PET image, an F-PET image, a T1-MRI image, an FA-DTI image and an MD-DTI image.
D13 [92]	18	MR, PET	18 patients (12 women, mean age 31.4 years, sd 5.6) and 10 age- and gender-matched healthy volunteers (8 women, mean age 29.4, sd 6.3).
D14 [116]	35	PET	24 patients diagnosed with AD and 11 patients as healthy control.
D15 [119]	74 pairs	NR (T1, T2), CT, PET	14 pairs of CT/MRI images, 20 pairs of MR-T1/MR-T2, 20 pairs of MR/SPECT, 20 pairs of MR/PET images.
D16 [2]	20	MR, CT	unpaired brain MR and CT image data volumes, including 179 two-dimensional (2D) axial MR and CT images.

Most deep learning model research need a huge amount of data due to the neural scaling law. Hence, it is an urgent issue that there is no enough data to support the research for cross-modality synthesis except for MRI-to-MRI synthesis. In addition, according to Fig 4, the size of MRI-to-MRI dataset is very small. The largest dataset, BraTS [8] only contains 3000 subjects. Most of MRI-to-MRI datasets contain no more than 500 data. Moreover, we can find that a lot of public MRI-to-MRI datasets have no labels for downstream tasks, like segmentation, classification, and so on. Since the aim

Table 5. A brief summary of different losses used in the reviewed publications (Part-I).

Abbr.	Function	Description
L_{gan}	$E_I[\log D(I)] + E_I[\log(1 - D(G(I)))]$	G and D are the generator and discriminator, respectively.
L_{cgan}	$E_{x,y}[\log D(x,y)] + E_{x,z}[\log(1 - D(x, G(x,z)))]$	Learn the transformation from conditioned sample $x \in X$ and random noise vector z to the desired output sample $y \in Y, G : \{x, z\} \rightarrow \{y\}$. The functions G and D are the outputs of the generator and discriminator respectively, and $E_{a,b}[f(x)]$ is the expectation value of $f(x)$ over the distributions of a, b .
L_{sgan}	$E_{y \sim \mathcal{Y}}[D_{\mathcal{Y}}(y)^2] + E_{x \sim \mathcal{X}}[(1 - D_{\mathcal{Y}}(G_{\mathcal{Y}}(x)))^2]$	G and D are the generator and discriminator, respectively.
L_{p2p}	$E_{x,y,z}[y - G(x,z) _1]$	In the context of image-to-image translation, low-frequency information is better captured when an l_1 penalty is added to the loss function. The l_1 term can be written as $ y - G(x,z) _1$.
L_{cont}	$E_{x \sim \rho}[\phi(G(x)) - \phi(x) _1]$	This loss is to ensure that the resulting data achieved from generator G retains the same content as the input versions. $\phi(\cdot)$ represents feature maps, and it adopts an l_1 distance to measure the cross-quality content loss.
L_{prec}	$E_{x,y}[V(y) - V(G(x)) _1]$	The perceptual loss is to ensure that the resulting data achieved from generator G retains the same content as the output versions. $V(\cdot)$ represents feature maps, and it adopts an l_1 distance to measure the cross-quality content loss. Incorporation of a perceptual loss during network training can yield visually more realistic results in computer vision tasks.
L_{text}	$\sum_I \ T_I(\phi(F(\tilde{I}^L)) - T_I(\phi(I^H)))\ _2^2$	A texture descriptor [83], involving several Gram matrices T_I .
L_{cyc}	$E_{x \sim A}[G_B(G_A(x)) - x _1] + E_{y \sim B}[G_A(G_B(y)) - y _1]$	Enforce forward-backward transformation consistency.
L_{seg}	$-\sum_i \log(\text{Seg}(G_i(x_i)))$	The segmentation loss is the weighted cross entropy loss. $\text{Seg}(\cdot)$ is the segmentation network.
L_{seg1}	$E_{x,c}[S(G(x,c), gt)]$	We concatenate the corresponding modality label c to the synthesized image as the input of the segmentation network S . gt is the ground truth of the tumor segmentation map.
L_{iden}	$E_{y \sim B}[G_{\mathcal{Y}}(y) - y _1]$	Identity consistency constraint, which can regularize the generator to preserve the colors and intensities during translation.
L_{rec1}	$E_{x \sim A, y \sim B, z \sim P(z)}[y - G(x,z) _1]$	The image y is reconstructed by generator G using the input x with the l_1 constrain. $P(z)$ is the standard normal distribution and $z \sim P(z)$ is the sampled latent vector.
L_{rec2}	$E_{x \sim A, y \sim B, z \sim P(z)}[y - G(x,z) _2]$	The same with L_{rec} . Here, it uses the l_2 constrain.
L_{kl}	$\mathbb{E}[D_{KL}(E(y)) N(0, 1)]$	To ensure the encoded vector has a similar distribution with the sampled latent vector, the KL-divergence constraint is enforced in the encoder network. It means that the difference between the encoded vector and the latent vector should be minimized. \mathbb{E} denotes expected value, E represents the encoder, D_{KL} denotes KL divergence, and z represents the latent vector sampled from the standard normal space.
L_{cla}	$L_{CE}(C(E(G(I_i, c_i), c_j), c_j)) + L_{CE}(C(E(I_i, c_i), c_i))$	Contrast-classification loss is to force classifier C to predict the contrast of extracted features by encoder E . We adversarially train the classifier to make deep features of multiple contrasts extracted by E to be same distributed, i.e., within a common feature space, using a gradient reversal layer in C , which flips gradient sign during backpropagation to force extracted deep features unable to be classified by C . L_{CE} computes the cross entropy between estimated contrast probability by C and real contrast code.
L_{cls}	$-y \log(x) - (1 - y) \log(1 - p(x))$	Universal cross-entropy loss. $p(x)$ is the estimated probability of x belonging to the correct class y .
L_{am}	$E_{p_a(x)}[(1 - M_x) \odot (G(x^a) - x^a) _2^2]$	For this medical imaging task in which accuracy is a major requirement of the model, the generator G needs to detect and modify the lesion region while keeping other parts unchanged. The L_{am} penalty is meant to enforce this, but to further help in this task we include a global shortcut to require the generator to learn a mapping that isolates and removes the lesion. M_x is mask of x . \odot represents element-wise multiplication and $\mathbf{1}$ is an all-ones matrix of the same size of the input image.
L_{fm}	$\sum_k \sum_i \frac{1}{N_i} \ D_k^i(x, y) - D_k^i(x, G(x))\ _2^2$	Feature matching loss is to stabilize training, which optimizes the generator to match these intermediate representations from the real and the synthesized images in multiple layers of the discriminators. D_k^i denotes the i th layer of the discriminator D_k , and N_i is the number of elements in the i th layer.
L_{sc}	$\text{GDL}(s, U(y)) + \text{GDL}(s, U(G(x)))$	Shape consistency loss is to regularize the generator to obey consistency relation. It adopts a generalized dice loss (GDL) [79] to measure the difference between the predicted and real segmentation maps. $U(y)$ and $U(G(x))$ represent the predicted lesion segmentation probability maps by taking y and $G(x)$ as inputs in the segmentation module, respectively. s denotes the ground truth lesion segmentation map.
L_{cm}	$c \otimes \hat{y} - y _1 - \lambda \sum_i \log(c^{ij})$	Confident map loss is to model the data dependent aleatoric uncertainty. \hat{y} is intermediate synthesis results of synthesized image y . c is the confidence map. To avoid a trivial solution (i.e. $c^{ij} = 0, \forall i, j$), λ is a constant adjusting the weight of this regularization term.

for cross-modality synthesis is to serve the downstream task, it is difficult to evaluate the real quality of synthesis neuroimage without the label for the downstream task. Most evaluation metrics, like PSNR, SSIM, are built on the basis of natural image space, which are not able to reflect the quality of cross-modality neuroimage. Thus, utilizing the performance of downstream task is a more powerful metric for cross-modality neuroimage synthesis [35].

4.2 Losses

Table 5 and Table 6 provide a comprehensive overview of the loss function in cross-modality neuroimage synthesis. The second column in Table 5 and Table 6 denotes the function of the loss. The third column describes the details or the

Table 6. A brief summary of different losses used in the reviewed publications (Part-II).

Abbr.	Function	Description
L_{dice}	$1 - \frac{1}{L} \sum_{l=1}^L \frac{\sum_p 2y_p(l)}{y_p(l)^2 + \sum_p y_p(l)^2}$	Dice loss [61] for accurate segmentation from multiple domain images, where L is the total number of classes, p is the spatial position index in the image, $\hat{y}(l)$ is the predicted segmentation probability map for class l from segmentation generator and $y(l)$ is the ground truth segmentation mask for class l .
L_{reg}	$E_{x \sim \mathcal{X}} [\ \mathcal{A}_{\mathcal{X}}(x)\mathcal{A}_{\mathcal{X}}(x)^T - 1\ _F] + E_{y \sim \mathcal{Y}} [\ \mathcal{A}_{\mathcal{X}}(G_{\mathcal{X}}(y))\mathcal{A}_{\mathcal{X}}(G_{\mathcal{X}}(y))^T - 1\ _F]$	Attention regularization loss term encourages the attention maps to be orthogonal with each other. \mathcal{A} the attention module. 1 is the identity matrix and $\ \cdot\ _F$ denotes the Frobenius norm.
L_{tiu}	$\frac{1}{n} \sum_{i=1}^n \frac{\sigma(p_i)}{\mu(p_i)} + \frac{1}{n} \sum_{i=1}^n \frac{\sigma(q_i)}{\mu(q_i)}$	To well handle the spatiotemporally-heterogeneous intensity changes of the brain MR images, L_{tiu} is designed to encourage the local intensity homogeneity in the corrected image. We assume that, for each brain tissue, i.e., gray matter (GM) and white matter (WM), the intensity values of the corrected image within a local patch are relatively homogeneous. p_i and q_j denote the i th and j th local patches sampled from the GM and WM of the "corrected" image, respectively. The operators $\sigma(\cdot)$ and $\mu(\cdot)$ are the standard deviation and mean, and $\sigma(\cdot)/\mu(\cdot)$ calculates the coefficient of variation for a local patch.
L_{cor}	$\gamma(1 - \kappa_{\zeta}(G(v), f))$	L_{cor} can more sensitively suppress the negative influence from the outliers or impulsive noises, and thus help stabilize the training procedure and consequently improve the quality of the bias fields. $\kappa_{\zeta}(G(v), f) = \exp(-\frac{(G(v)-f)^2}{2\zeta^2})$ is the Gaussian kernel, ζ is the corresponding tuning bandwidth, and $\gamma = (1 - \exp(-\frac{1}{2\zeta^2}))^{-1}$.
L_{sm}	$\ \Delta G(v)\ _2^2$	The bias fields $G(v)$ estimated from the input intensity images should be smooth. A smoothness loss function is based on the Laplacian operator to provide explicit guidance of the smoothness constraint.
L_{ssim}	$-\log(\frac{1}{2 P } \sum_{p \in P} (1 + SSIM(p)))$	Structural similarity index loss. P denotes the pixel location set and $ P $ is its cardinality. $SSIM(\cdot)$ is one of the perceptual metrics and it is also differentiable.
L_{mc}	$E_{\sim \hat{x}_y} [-\log(D(\hat{x}_y, m_y))] + E_{\sim x} [-\log(D(x, m_x))]$	Modality classification loss. Given the pair of input sample and target modality x, m_y , we propose to learn a parameterized mapping $f: x, m_y \rightarrow \hat{x}_y$ from x, m_y to the generated corresponding sample with modality m_y to closely resemble x_y . m_y denotes a four-dimensional one-hot vector to represent the four MR modalities
L_{gdl}	Gradient difference loss	To deal with the inherently blurry effect.
L_{edge}	Edge-aware constraint	Based on the similarity of the edge maps from synthesized and real images.
L_{tumor}	Tumor-aware constraint	The edge-aware learning helps the model capture the context information of the entire brain, but not necessarily for individual tumors. Since tumor appearance is highly variable and subject-specific, it is hard to synthesize than the normal tissue.
L_{mani}	Manifold regularizer	To preserve the complementary properties. Since image manifold reflects the intrinsic geometric structure underlying the data leading to the generated results with a realistic overall structure.
L_{mmd}	Regularization	Maximum mean discrepancy regularization [16].
L_{gcr}	Regularization	Geometry co-regularization.
L_{ae}	Reconstruction	Autoencoder reconstruction.
L_{oth}	Regularization	Spectral restricted isometry property regularization [4].
L_{fault}	Fault-aware discriminator	To make the synthesized results can satisfy the requirement of segmentation and substitute the real acquisitions in practice, and bridge the gap of segmentation performance between synthesized data and real ones.

role of the loss function. We category the overall loss functions into four streams. The first stream is the reconstruction loss function, including identity loss function L_{iden} , pixel loss function L_{p2p} , the edge loss function L_{edge} , the tumor loss function L_{tumor} , the rectification loss function L_{rec1} and L_{rec2} and the feature matching loss function L_{fm} . All of them propose to add the constraint into the reconstruction process, no matter it is in the pixel space or the feature space. The second type of loss function is strongly related to the downstream task, like segmentation loss L_{seg} , dice score loss L_{dice} , cross entropy loss L_{cls} and modality classification loss L_{mc} . These loss functions aim to jointly optimize the downstream task with cross-modality neuroimage synthesis. The third loss function is regularizer loss function. For instance, L_{mmd} is the maximum discrepancy regularization when seeking the paired feature points from the source modality neuroimage and the target modality neuroimage. L_{cor} stabilizes the training procedure and improve the quality of the bias field by suppressing the negative influence from the outlier noise.

4.3 Metrics

Table 7 offers a comprehensive review of the metrics in cross-modality neuroimage synthesis. The first column denotes the name of the metric and the second column denotes the level. In other words, if the level is up, it means the larger the metrics value is, the better the performance. If the level is down, it means the metrics value is lower, the performance is better. The third column gives the detail for each metric, especially on how the metric accurately

Table 7. A brief summary of different metrics used in the reviewed publications.

Abbr.	Level	Metric	Description
PSNR	↑	Peak signal-to-noise ratio	
SSIM	↑	Structural similarity	
MSSSIM	↑	Multiscale structural similarity	
MAE	↓	Mean absolute error	
DSC	↑	Dice similarity coefficient	DSC is employed to evaluate different approaches by comparing their segmentation results against the ground truth voxel-by-voxel. Differences between methods are evaluated by Wilcoxon signed rank test [94] with a significance threshold of $p < 0.05$.
ASD/ASSD	↑	Average (symmetric) surface distance	ASD is used to compute the average surface distance from y_{pred} to y under the default setting. This tell us how much, on average, the surface varies between the segmentation and the GT.
MOS	↑	Mean opinion score	measures the quality of a given image by a rating score between 1 and 5: 1 indicates inferior while 5 indicates superior.
DS	↓	Deformation score	DS is registration metric based on Jacobian. For the DS, an FFD-based [72] deformable registration was applied to the synthesised MR to register to a real MR at a similar imaging plane. The average Jacobian (normalised to [0,1]) of the required deformation to complete such registration was computed as the score consequently. The underlying assumption is that a synthesised MRI with high quality tends to have a lower Jacobian when registering to the real MRI.
P	↑	Precision	The fraction of true positive examples among the examples that the model classified as positive.
R	↑	Recall	The fraction of examples classified as positive, among the total number of positive examples.
F1S	↑	F1 score for classification	It is defined as $2(P \times R)/(P + R)$.
F-score	↑	F1 score for segmentation	Measure the overlap of ground truth segmentation labels. It is defined as $(2 H \cap G)/(H + G)$ where G is the label of the target image and H is the prediction of the source image.
VS	↑	Verisimilitude score	A higher VS means more produced pseudo-healthy images fool the classifier successfully, indicating the model can better generate lesion-free images lying in the true data distribution of normal images.
MSE	↓	Mean-squared error	
NMSE	↓	Normalized mean-squared error	
RMSE	↓	Root mean-squared error	
NRMSE	↓	Normalized root mean-squared error	
HD95	↓	95th Hausdorff Distance	Between obtained tissue segmentation maps and manually-corrected tissue segmentation maps were .
CC	↓	Correlation coefficient	between the estimated bias field and the ground-truth bias field [82].
CIV	↑	Coefficient of intensity variation	For each tissue [15].
L1	↓	L1 error	global image L1.
L2	↓	L2 error	global image L2.
t-L2	↓	Tumor-averaged L2	Based on segmentation maps of enhancing lesions.
FID	↓	Fréchet inception distance	For the evaluation of the performance of GANs at image generation [24].
UQI	↑	Universal quality index	This index is designed by modeling any image distortion as a combination of three factors: loss of correlation, luminance distortion, and contrast distortion [90].
MMD	↓	Maximum mean discrepancy	In terms of particular function spaces that witness the difference in distributions [16].
IS	↑	Inception score	
ACC	↑	Accuracy	
AUC	↑	Area under curve	Area under the receiver operating characteristic.
ROC	↑	Receiver operator characteristic	Show the diagnostic ability of binary classifiers.
BAC	↑	Balanced accuracy	
SEN	↑	Sensitivity	
SPE	↑	Specificity	
MCC	↑	Matthews correlation coefficient	[58]
DVR	↑	[¹¹ C]PIB PET distribution volume ratio	Select the myelin content.
MI	↑	Mutual information	[91]
Q	↑	Weighted fusion quality metric	[69]
FMI	↑	Feature mutual information measures	[18]

indicate the synthesis quality of cross-modality neuroimage on certain circumstance. From Table 7, it can be easily observed that most of novel metrics are the variants of traditional shallow reference metrics, such as MAE, PSNR or SSIM. However, these metrics can not correspond to the quality of neuroimage. Because they focus more on the blurriness of the neuroimage and disregard its fundamental traits, such as the structural characteristics of the lesion area and the k-space feature drift. One alternative approach to alleviate this problem is to use downstream tasks such as segmentation or classification to validate the quantity of generated samples. But this approach cannot be seamlessly

integrated into end-to-end optimization manner for cross-modality neuroimage synthesis. The hiring of radiologist for review is another option, but it is too costly, time-consuming, and difficult to scale up. Hence, the validity of these metrics for neuroimages remains to be explored.

5 OPEN CHALLENGES AND FUTURE DIRECTIONS

As an emerging area, research on multi-modality brain image synthesis is still in its infancy stage. The challenging topics required to be investigated are summarized as follows.

Challenge 1: Jointly optimize synthesis model and downstream Task. How to jointly optimize the cross-modality neuroimage synthesis and the downstream tasks with either weakly-supervised or unsupervised learning? Previously, neuroimage synthesis [37, 76] is generally regarded as a standalone task, which overlooks one important fact, namely whether the synthesized results can improve the downstream tasks. Recently, there have been improvement in jointly optimizing cross-modality neuroimage synthesis and downstream tasks. The unsupervised learning methods [20, 80, 107] and the weakly-supervised learning approaches [75, 115] start to pay attention to the downstream tasks rather than focusing on the quality of synthesized results only.

Future direction: Multi-task learning. Transforming downstream task and cross-modality synthesis into a multi-task learning issue improves both the synthesis quality of cross-modality neuroimages and the performance of downstream task.

Challenge 2: Correctness of synthesized lesions. How to ensure the correctness of the synthesized lesions? Previously, most of the cross-modality image synthesis algorithms pay attention to the whole image quality, which fails to highlight the more important disease-related regions (see Fig. 3).

Future direction: Lesion-oriented synthesis. The method reported in [80] provides a potential answer to this question since the lesion diagnosis can be treated as an anomaly detection problem. If we can detect the disease region and use it as the guidance for cross-modality brain image synthesis, the generated output is given in a disease-highlighted and lesion-oriented manner.

Challenge 3: Evaluation metric. How to build up an appropriate metric to evaluate the results of cross-modality image synthesis? The existing measurements are evaluated by PSNR and SSIM, which are established on natural images but ignore the inherent properties of neuroimage. The translated medical data with highest PSNR or SSIM may be still blurred or important tissue representations that should be correctly highlighted are missing.

Future direction: K-space-aware metrics. The k-space imaging concept is the main distinction between MR imaging and natural pictures, other than the disease area. The critical lesion location and essential k-space specialty of neuroimages should be accurately reflected by the new metric for synthetic quality. Therefore, the new metric should encompass the lesion region, k-space characteristics, and anatomical features.

Challenge 4: Misaligned data usage. How to utilize the misaligned neuroimaging data for cross-modality image synthesis? In practice, there exists a large amount of misaligned neuroimaging data in each vendor (i.e., hospital). The state-of-the-art image registration algorithm takes plenty of time for each misaligned brain image. It requires huge amount of laborious work to verify the effect of the registration algorithm. It is questionable whether the strong dependence on registration and full utilization of misaligned data can be eliminated for cross-modality synthesis.

Future direction: Misaligned neuroimage as data augmentation. Kong *et al.* [46] and Xie *et al.* [96] attempt to eliminate the need of registration and make full use of the misaligned neuroimaging data for synthesis. The work of [46] incorporate the correction loss into CycleGAN [118], while Wang *et al.* [86] regard the misaligned neuroimaging data as a data augmentation of self-supervised learning method and design an affined transform loss to let the discriminator

overcoming the over-fitting problem. Furthermore, the authors in [86] stimulate the severe misaligned neuroimaging data and find out that their methods perform better in severe misaligned condition.

Challenge 5: A unified model. How to build up a unified model for cross-modality brain image synthesis? Previously, most work pay attention to various modality synthesis in MR, CT and PET. Charts *et al.* [8] propose a multi-input and multi-output fully convolutional network model to synthesize various modalities of MRI. Similar with the work of [8], Liu *et al.* [53] propose a unified conditional disentanglement work to synthesize various modality of MRI. However, a simultaneous work for synthesizing varying modality among MR, CT and PET lacks.

Future direction: One to many via invariant features This topic may have a solution in the work of [116], which uses a cycle-consistent GAN to extract the invariant features from various modalities. Nevertheless, its synthesis range is limited in MRI-to-MRI. The invariant characteristics from CT, PET, and MRI should be extracted in order to train a uniform synthesis model in the future.

Challenge 6: Data privacy. How to solve the data isolation problems while protecting the patients' privacy for cross-modality brain image synthesis? The current state-of-the-art brain image synthesis algorithms just consider a centralized training strategy. However, many medical institutions cannot share their data, which is restricted by the privacy protection legislation.

Future direction: Federated cross-modality neuroimage synthesis. Xie *et al.* [95] is the first one to solve this question. However, the authors do not consider the downstream task with the synthesized neuroimaging data. In this sector, there are still several opportunities for advancement.

6 CONCLUSION

In this paper, we provide a literature review on cross-modality brain image synthesis, focusing on the level of supervision, the improvement for the downstream task, the types of synthesis modalities, the types and properties of datasets, the roles of the loss function, and the evaluation metrics for neuroimage quality. In particular, we characterize the architecture of existing cross-modality synthesis models based on the supervision level. In addition, for each downstream task, we analyze in detail how cross-modality neuroimage synthesis enhances its performance. In the end, we highlight a number of exciting future research directions for cross-modality neuroimage synthesis.

ACKNOWLEDGMENTS

This work is supported by the National Natural Science Foundation of China under Grant No. 61972188, 62122035, and 62206122.

REFERENCES

- [1] Michal Aharon, Michael Elad, Alfred Marcel Bruckstein, and Y. Katz. 2005. K-SVD : An Algorithm for Designing of Overcomplete Dictionaries for Sparse Representation.
- [2] Omar S Al-Kadi, Israa Almallahi, Alaa Abu-Srhan, AM Mohammad Abushariah, and Waleed Mahafza. 2022. Unpaired MR-CT brain dataset for unsupervised image translation. *Data in Brief* 42 (2022), 108109.
- [3] Paul Aljabar, Robin Wolz, Latha Srinivasan, Serena J. Counsell, Mary A. Rutherford, Anthony David Edwards, Joseph V. Hajnal, and Daniel Rueckert. 2011. A Combined Manifold Learning Analysis of Shape and Appearance to Characterize Neonatal Brain Development. *IEEE Transactions on Medical Imaging* 30 (2011), 2072–2086.
- [4] Nitin Bansal, Xiaohan Chen, and Zhangyang Wang. 2018. Can we gain more from orthogonality regularizations in training deep networks? *Advances in Neural Information Processing Systems* 31 (2018).
- [5] Xuesheng Bian, Xiongbiao Luo, Cheng Wang, Weiyan Liu, and Xiuhong Lin. 2022. DDA-Net: Unsupervised cross-modality medical image segmentation via dual domain adaptation. *Computer Methods and Programs in Biomedicine* 213 (2022), 106531.

- [6] Alexandre Bône, Samy Ammari, Jean-Philippe Lamarque, Mickael Elhaik, Émilie Chouzenoux, François Nicolas, Philippe Robert, Corinne Balleyguier, Nathalie Lassau, and Marc-Michel Rohé. 2021. Contrast-Enhanced Brain MRI Synthesis With Deep Learning: Key Input Modalities and Asymptotic Performance. *2021 IEEE 18th International Symposium on Biomedical Imaging (ISBI)* (2021), 1159–1163.
- [7] Agisilaos Chartsias, Thomas Joyce, Mario Valerio Giuffrida, and Sotirios A Tsafaris. 2017. Multimodal MR synthesis via modality-invariant latent representation. *IEEE transactions on medical imaging* 37, 3 (2017), 803–814.
- [8] Agisilaos Chartsias, Thomas Joyce, Mario Valerio Giuffrida, and Sotirios A. Tsafaris. 2018. Multimodal MR Synthesis via Modality-Invariant Latent Representation. *IEEE Transactions on Medical Imaging* 37 (2018), 803–814.
- [9] Cheng Chen, Qi Dou, Hao Chen, and Pheng-Ann Heng. 2018. Semantic-Aware Generative Adversarial Nets for Unsupervised Domain Adaptation in Chest X-ray Segmentation. In *MLMI@MICCAI*.
- [10] Cheng Chen, Qi Dou, Hao Chen, Jing Qin, and Pheng-Ann Heng. 2020. Unsupervised Bidirectional Cross-Modality Adaptation via Deeply Synergistic Image and Feature Alignment for Medical Image Segmentation. *IEEE Transactions on Medical Imaging* 39 (2020), 2494–2505.
- [11] Liangjun Chen, Zhengwang Wu, Dan Hu, Fan Wang, J. Keith Smith, Weili Lin, Li Wang, Dinggang Shen, and Gang Li. 2021. ABCnet: Adversarial bias correction network for infant brain MR images. *Medical image analysis* 72 (2021), 102133.
- [12] Zekang Chen, Jia Wei, and Rui Li. 2022. Unsupervised Multi-Modal Medical Image Registration via Discriminator-Free Image-to-Image Translation. In *IJCAI*.
- [13] Salman Ul Hassan Dar, Mahmut Yurt, Levent Karacan, Aykut Erdem, Erku Erdem, and Tolga Çukur. 2019. Image Synthesis in Multi-Contrast MRI With Conditional Generative Adversarial Networks. *IEEE Transactions on Medical Imaging* 38 (2019), 2375–2388.
- [14] Kathryn A Ellis, Ashley I Bush, David Darby, Daniela De Fazio, Jonathan Foster, Peter Hudson, Nicola T Lautenschlager, Nat Lenzo, Ralph N Martins, Paul Maruff, et al. 2009. The Australian Imaging, Biomarkers and Lifestyle (AIBL) study of aging: methodology and baseline characteristics of 1112 individuals recruited for a longitudinal study of Alzheimer’s disease. *International psychogeriatrics* 21, 4 (2009), 672–687.
- [15] Maryjo M George, S Kalaivani, and MS Sudhakar. 2017. A non-iterative multi-scale approach for intensity inhomogeneity correction in MRI. *Magnetic Resonance Imaging* 42 (2017), 43–59.
- [16] Arthur Gretton, Karsten M Borgwardt, Malte J Rasch, Bernhard Schölkopf, and Alexander Smola. 2012. A kernel two-sample test. *The Journal of Machine Learning Research* 13, 1 (2012), 723–773.
- [17] Pengfei Guo, Puyang Wang, Rajeev Yasarla, Jinyuan Zhou, Vishal M. Patel, and Shanshan Jiang. 2021. Anatomic and Molecular MR Image Synthesis Using Confidence Guided CNNs. *IEEE Transactions on Medical Imaging* 40 (2021), 2832–2844.
- [18] Mohammad Haghghat and Masoud Amirkabiri Razian. 2014. Fast-FMI: Non-reference image fusion metric. In *2014 IEEE 8th International Conference on Application of Information and Communication Technologies (AICT)*. IEEE, 1–3.
- [19] Xiao Han. 2017. MR-based synthetic CT generation using a deep convolutional neural network method. *Medical Physics* 44 (2017), 1408–1419.
- [20] Yufan He, Aaron Carass, Lianrui Zuo, Blake E. Dewey, and Jerry L Prince. 2021. Autoencoder based self-supervised test-time adaptation for medical image analysis. *Medical image analysis* 72 (2021), 102136.
- [21] Yuan He, Aoyu Wang, Shuai Li, Yikang Yang, and Aimin Hao. 2022. Nonfinite-modality data augmentation for brain image registration. *Computers in biology and medicine* 147 (2022), 105780.
- [22] Rolf A. Heckemann, Joseph V. Hajnal, Paul Aljabar, Daniel Rueckert, and Alexander Hammers. 2006. Automatic anatomical brain MRI segmentation combining label propagation and decision fusion. *NeuroImage* 33 (2006), 115–126.
- [23] Matt Hemsley, Brige P. Chugh, Mark Ruschin, Young Lee, Chia-Lin Tseng, Greg J. Stanisz, and Angus Z. Lau. 2020. Deep Generative Model for Synthetic-CT Generation with Uncertainty Predictions. In *MICCAI*.
- [24] Martin Heusel, Hubert Ramsauer, Thomas Unterthiner, Bernhard Nessler, and Sepp Hochreiter. 2017. Gans trained by a two time-scale update rule converge to a local nash equilibrium. *Advances in neural information processing systems* 30 (2017).
- [25] Yuta Hiasa, Yoshito Otake, Masaki Takao, Takumi Matsuoka, Kazuma Takashima, Jerry L Prince, Nobuhiko Sugano, and Yoshinobu Sato. 2018. Cross-modality image synthesis from unpaired data using CycleGAN: Effects of gradient consistency loss and training data size. *ArXiv abs/1803.06629* (2018).
- [26] Brittany R Howell, Martin A Styner, Wei Gao, Pew-Thian Yap, Li Wang, Kristine Baluyot, Essa Yacoub, Geng Chen, Taylor Potts, Andrew Salzwedel, et al. 2019. The UNC/UMN Baby Connectome Project (BCP): An overview of the study design and protocol development. *NeuroImage* 185 (2019), 891–905.
- [27] Shengye Hu, Baiying Lei, Shuqiang Wang, Yong Wang, Zhiguang Feng, and Yanyan Shen. 2022. Bidirectional Mapping Generative Adversarial Networks for Brain MR to PET Synthesis. *IEEE Transactions on Medical Imaging* 41 (2022), 145–157.
- [28] Shengye Hu, Yanyan Shen, Shuqiang Wang, and Baiying Lei. 2020. Brain MR to PET Synthesis via Bidirectional Generative Adversarial Network. In *MICCAI*.
- [29] Pu Huang, Dengwang Li, Zhicheng Jiao, Dongming Wei, Guoshi Li, Qian Wang, Han Zhang, and Dinggang Shen. 2019. CoCa-GAN: Common-Feature-Learning-Based Context-Aware Generative Adversarial Network for Glioma Grading. In *MICCAI*.
- [30] Yawen Huang, Leandro Beltrachini, Ling Shao, and Alejandro F Frangi. 2016. Geometry Regularized Joint Dictionary Learning for Cross-Modality Image Synthesis in Magnetic Resonance Imaging. In *SASHIMI@MICCAI*.
- [31] Yawen Huang, Ling Shao, and Alejandro F. Frangi. 2017. DOTE: Dual cOnvolutional filTer LEarning for Super-Resolution and Cross-Modality Synthesis in MRI. In *MICCAI*.

- [32] Yawen Huang, Ling Shao, and Alejandro F. Frangi. 2017. Simultaneous Super-Resolution and Cross-Modality Synthesis of 3D Medical Images Using Weakly-Supervised Joint Convolutional Sparse Coding. *2017 IEEE Conference on Computer Vision and Pattern Recognition (CVPR)* (2017), 5787–5796.
- [33] Yawen Huang, Ling Shao, and Alejandro F. Frangi. 2018. Cross-Modality Image Synthesis via Weakly Coupled and Geometry Co-Regularized Joint Dictionary Learning. *IEEE Transactions on Medical Imaging* 37 (2018), 815–827.
- [34] Yawen Huang, Ling Shao, and Alejandro F. Frangi. 2019. Simultaneous Super-Resolution and Cross-Modality Synthesis in Magnetic Resonance Imaging. In *Deep Learning and Convolutional Neural Networks for Medical Imaging and Clinical Informatics*.
- [35] Yawen Huang, Feng Zheng, Runmin Cong, Weilin Huang, Matthew R. Scott, and Ling Shao. 2020. MCMT-GAN: Multi-Task Coherent Modality Transferable GAN for 3D Brain Image Synthesis. *IEEE Transactions on Image Processing* 29 (2020), 8187–8198.
- [36] Yawen Huang, Feng Zheng, Danyang Wang, Junyu Jiang, Xiaoqian Wang, and Ling Shao. 2020. Super-Resolution and Inpainting with Degraded and Upgraded Generative Adversarial Networks. In *IJCAI*.
- [37] Yuankai Huo, Zhoubing Xu, Hyeonsoo Moon, Shunxing Bao, Albert Assad, Tamara K. Moyo, Michael R. Savona, Richard G. Abramson, and Bennett A. Landman. 2019. SynSeg-Net: Synthetic Segmentation Without Target Modality Ground Truth. *IEEE Transactions on Medical Imaging* 38 (2019), 1016–1025.
- [38] Tri Huynh, Yaorong Gao, Jiayin Kang, Li Wang, Pei Zhang, Jun Lian, and Dinggang Shen. 2015. Estimating CT image from MRI data using structured random forest and auto-context model. *IEEE transactions on medical imaging* 35, 1 (2015), 174–183.
- [39] Phillip Isola, Jun-Yan Zhu, Tinghui Zhou, and Alexei A. Efros. 2017. Image-to-Image Translation with Conditional Adversarial Networks. *2017 IEEE Conference on Computer Vision and Pattern Recognition (CVPR)* (2017), 5967–5976.
- [40] Clifford R Jack Jr, Matt A Bernstein, Nick C Fox, Paul Thompson, Gene Alexander, Danielle Harvey, Bret Borowski, Paula J Britson, Jennifer L. Whitwell, Chadwick Ward, et al. 2008. The Alzheimer’s disease neuroimaging initiative (ADNI): MRI methods. *Journal of Magnetic Resonance Imaging: An Official Journal of the International Society for Magnetic Resonance in Medicine* 27, 4 (2008), 685–691.
- [41] Jianbo Jiao, Ana I. L. Namburete, Aris T. Papageorghiou, and Julia Alison Noble. 2020. Self-Supervised Ultrasound to MRI Fetal Brain Image Synthesis. *IEEE Transactions on Medical Imaging* 39 (2020), 4413–4424.
- [42] Amod Jog, Aaron Carass, Snehashis Roy, Dzung L. Pham, and Jerry L Prince. 2017. Random forest regression for magnetic resonance image synthesis. *Medical Image Analysis* 35 (2017), 475–488.
- [43] Thomas Joyce, Agisilaos Chartsias, and Sotirios A. Tsaftaris. 2017. Robust Multi-modal MR Image Synthesis. In *MICCAI*.
- [44] Chia-Hsiang Kao, Yong-Sheng Chen, Li-Fen Chen, and Wei-Chen Chiu. 2021. Demystifying T1-MRI to FDG¹⁸-PET Image Translation via Representational Similarity. In *International Conference on Medical Image Computing and Computer-Assisted Intervention*. Springer, 402–412.
- [45] Kerstin Kläser, Thomas Varsavsky, Pawel J. Markiewicz, Tom Kamiel Magda Vercauteren, Alexander Hammers, David Atkinson, K. Thielemans, Brian F. Hutton, Manuel Jorge Cardoso, and Sébastien Ourselin. 2021. Imitation learning for improved 3D PET/MR attenuation correction. *Medical Image Analysis* 71 (2021).
- [46] Lingke Kong, Chenyu Lian, Detian Huang, Zhenjiang Li, Yanle Hu, and Qichao Zhou. 2021. Breaking the Dilemma of Medical Image-to-image Translation. *ArXiv abs/2110.06465* (2021).
- [47] Gihyun Kwon, Chihye Han, and Dae-Shik Kim. 2019. Generation of 3D Brain MRI Using Auto-Encoding Generative Adversarial Networks. In *MICCAI*.
- [48] Bennett A Landman, Alan J Huang, Aliya Gifford, Deepti S Vikram, Issel Anne L Lim, Jonathan AD Farrell, John A Bogovic, Jun Hua, Min Chen, Samson Jarso, et al. 2011. Multi-parametric neuroimaging reproducibility: a 3-T resource study. *Neuroimage* 54, 4 (2011), 2854–2866.
- [49] Dongwook Lee, Junyoung Kim, Won-Jin Moon, and J. C. Ye. 2019. CollaGAN: Collaborative GAN for Missing Image Data Imputation. *2019 IEEE/CVF Conference on Computer Vision and Pattern Recognition (CVPR)* (2019), 2482–2491.
- [50] Hongwei Li, Johannes C. Paetzold, Anjany Kumar Sekuboyina, Florian Kofler, Jianguo Zhang, Jan S. Kirschke, Benedikt Wiestler, and Bjoern H. Menze. 2019. DiamondGAN: Unified Multi-Modal Generative Adversarial Networks for MRI Sequences Synthesis. *ArXiv abs/1904.12894* (2019).
- [51] Sook-Lei Liew, Julia M Anglin, Nick W Banks, Matt Sondag, Kaori L Ito, Hosung Kim, Jennifer Chan, Joyce Ito, Connie Jung, Nima Khoshab, et al. 2018. A large, open source dataset of stroke anatomical brain images and manual lesion segmentations. *Scientific data* 5, 1 (2018), 1–11.
- [52] Geert Litjens, Oscar Debats, Jelle Barentsz, Nico Karssemeijer, and Henkjan Huisman. 2014. Computer-aided detection of prostate cancer in MRI. *IEEE transactions on medical imaging* 33, 5 (2014), 1083–1092.
- [53] Xiaofeng Liu, Fangxu Xing, Georges El Fakhri, and Jonghye Woo. 2021. A Unified Conditional Disentanglement Framework For Multimodal Brain Mr Image Translation. *2021 IEEE 18th International Symposium on Biomedical Imaging (ISBI)* (2021), 10–14.
- [54] Yunbi Liu, Ling Yue, Shifu Xiao, Wei Yang, Dinggang Shen, and Mingxia Liu. 2022. Assessing clinical progression from subjective cognitive decline to mild cognitive impairment with incomplete multi-modal neuroimages. *Medical image analysis* 75 (2022), 102266.
- [55] Frederik Maes, André M. F. Collignon, Dirk Vandermeulen, Guy Marchal, and Paul Suetens. 1997. Multimodality image registration by maximization of mutual information. *IEEE Transactions on Medical Imaging* 16 (1997), 187–198.
- [56] Oskar Maier, Bjoern H Menze, Janina von der Gablentz, Levin Häni, Mattias P Heinrich, Matthias Liebrand, Stefan Winzeck, Abdul Basit, Paul Bentley, Liang Chen, et al. 2017. ISLES 2015-A public evaluation benchmark for ischemic stroke lesion segmentation from multispectral MRI. *Medical image analysis* 35 (2017), 250–269.
- [57] M. Maspero, Mark Savenije, Anna M. Dinkla, Peter R. Seevinck, Martijn P W Intven, Ina M Jurgenliemk-Schulz, Linda G. W. Kerkmeijer, and Cornelis A. T. van den Berg. 2018. Dose evaluation of fast synthetic-CT generation using a generative adversarial network for general pelvis MR-only radiotherapy. *Physics in Medicine & Biology* 63 (2018).

- [58] Brian W Matthews. 1975. Comparison of the predicted and observed secondary structure of T4 phage lysozyme. *Biochimica et Biophysica Acta (BBA)-Protein Structure* 405, 2 (1975), 442–451.
- [59] Adrienne M Mendrik, Koen L Vincken, Hugo J Kuijf, Marcel Breeuwer, Willem H Bouvy, Jeroen De Bresser, Amir Alansary, Marleen De Bruijne, Aaron Carass, Ayman El-Baz, et al. 2015. MRBrainS challenge: online evaluation framework for brain image segmentation in 3T MRI scans. *Computational intelligence and neuroscience* (2015).
- [60] Bjoern H Menze, Andras Jakab, Stefan Bauer, Jayashree Kalpathy-Cramer, Keyvan Farahani, Justin Kirby, Yuliya Burren, Nicole Porz, Johannes Slotboom, Roland Wiest, et al. 2014. The multimodal brain tumor image segmentation benchmark (BRATS). *IEEE transactions on medical imaging* 34, 10 (2014), 1993–2024.
- [61] Fausto Milletari, Nassir Navab, and Seyed-Ahmad Ahmadi. 2016. V-net: Fully convolutional neural networks for volumetric medical image segmentation. In *2016 fourth international conference on 3D vision (3DV)*. IEEE, 565–571.
- [62] Hien Van Nguyen, Shaohua Kevin Zhou, and Raviteja Vemulapalli. 2015. Cross-Domain Synthesis of Medical Images Using Efficient Location-Sensitive Deep Network. In *International Conference on Medical Image Computing and Computer-Assisted Intervention*.
- [63] Dong Nie, Roger Trullo, Caroline Petitjean, Su Ruan, and Dinggang Shen. 2017. Medical Image Synthesis with Context-Aware Generative Adversarial Networks. *Medical image computing and computer-assisted intervention : MICCAI ... International Conference on Medical Image Computing and Computer-Assisted Intervention* 10435 (2017), 417–425.
- [64] Sahin Olut, Yusuf Huseyin Sahin, Ugur Demir, and Gözde B. Ünal. 2018. Generative Adversarial Training for MRA Image Synthesis Using Multi-Contrast MRI. In *PRIME@MICCAI*.
- [65] Yongsheng Pan, Mingxia Liu, Chunfeng Lian, Yong Xia, and Dinggang Shen. 2019. Disease-Image Specific Generative Adversarial Network for Brain Disease Diagnosis with Incomplete Multi-modal Neuroimages. In *MICCAI*.
- [66] Yongsheng Pan, Mingxia Liu, Chunfeng Lian, Tao Zhou, Yong Xia, and Dinggang Shen. 2018. Synthesizing Missing PET from MRI with Cycle-consistent Generative Adversarial Networks for Alzheimer’s Disease Diagnosis. *Medical image computing and computer-assisted intervention : MICCAI ... International Conference on Medical Image Computing and Computer-Assisted Intervention* 11072 (2018), 455–463.
- [67] Yongsheng Pan, Mingxia Liu, Yong Xia, and Dinggang Shen. 2021. Disease-image-specific Learning for Diagnosis-oriented Neuroimage Synthesis with Incomplete Multi-Modality Data. *IEEE transactions on pattern analysis and machine intelligence* PP (2021).
- [68] Yongsheng Pan, Mingxia Liu, Yong Xia, and Dinggang Shen. 2021. Disease-image-specific learning for diagnosis-oriented neuroimage synthesis with incomplete multi-modality data. *IEEE Transactions on Pattern Analysis and Machine Intelligence* (2021).
- [69] Gemma Piella and Henk Heijmans. 2003. A new quality metric for image fusion. In *Proceedings 2003 international conference on image processing (Cat. No. 03CH37429)*, Vol. 3. IEEE, III–173.
- [70] Yili Qu, Chufu Deng, Wanqi Su, Ying Wang, Yutong Lu, and Zhiguang Chen. 2020. Multimodal brain MRI translation focused on lesions. In *Proceedings of the 2020 12th international conference on machine learning and computing*. 352–359.
- [71] Snehashis Roy, Aaron Carass, and Jerry L Prince. 2013. Magnetic Resonance Image Example-Based Contrast Synthesis. *IEEE Transactions on Medical Imaging* 32 (2013), 2348–2363.
- [72] Daniel Rueckert, Luke I Sonoda, Carmel Hayes, Derek LG Hill, Martin O Leach, and David J Hawkes. 1999. Nonrigid registration using free-form deformations: application to breast MR images. *IEEE transactions on medical imaging* 18, 8 (1999), 712–721.
- [73] Ramprasaath R. Selvaraju, Abhishek Das, Ramakrishna Vedantam, Michael Cogswell, Devi Parikh, and Dhruv Batra. 2019. Grad-CAM: Visual Explanations from Deep Networks via Gradient-Based Localization. *International Journal of Computer Vision* 128 (2019), 336–359.
- [74] Anmol Sharma and G. Hamarneh. 2020. Missing MRI Pulse Sequence Synthesis Using Multi-Modal Generative Adversarial Network. *IEEE Transactions on Medical Imaging* 39 (2020), 1170–1183.
- [75] Liyue Shen, Wentao Zhu, Xiaosong Wang, Lei Xing, John M. Pauly, Baris Turkbey, Stephanie A. Harmon, Thomas Sanford, Sherif Mehralivand, Peter L. Choyke, Bradford J. Wood, and Daguang Xu. 2021. Multi-Domain Image Completion for Random Missing Input Data. *IEEE Transactions on Medical Imaging* 40 (2021), 1113–1122.
- [76] Hoo-Chang Shin, Alvin Ihsani, Ziyue Xu, Swetha Mandava, Sharath Turuvekere Sreenivas, Christopher Forster, Jiok Cha, and Alzheimer’s Disease Neuroimaging Initiative. 2020. GANDALF: Generative Adversarial Networks with Discriminator-Adaptive Loss Fine-tuning for Alzheimer’s Disease Diagnosis from MRI. In *MICCAI*.
- [77] Md Mahfuzur Rahman Siddiquee, Zongwei Zhou, Nima Tajbakhsh, Ruibin Feng, Michael B. Gotway, Yoshua Bengio, and Jianming Liang. 2019. Learning Fixed Points in Generative Adversarial Networks: From Image-to-Image Translation to Disease Detection and Localization. *2019 IEEE/CVF International Conference on Computer Vision (ICCV)* (2019), 191–200.
- [78] Rebecca L. Siegel, Kimberly D Miller, and Ahmedin Jemal. 2019. Cancer statistics, 2019. *CA: A Cancer Journal for Clinicians* 69 (2019).
- [79] Carole H Sudre, Wenqi Li, Tom Vercauteren, Sebastien Ourselin, and M Jorge Cardoso. 2017. Generalised dice overlap as a deep learning loss function for highly unbalanced segmentations. In *Deep learning in medical image analysis and multimodal learning for clinical decision support*. Springer, 240–248.
- [80] Liyan Sun, Jiexiang Wang, Yue Huang, Xinghao Ding, Hayit Greenspan, and John William Paisley. 2020. An Adversarial Learning Approach to Medical Image Synthesis for Lesion Detection. *IEEE Journal of Biomedical and Health Informatics* 24 (2020), 2303–2314.
- [81] Devavrat Tomar, Manana Lortkipanidze, Guillaume Vray, Behzad Bozorgtabar, and Jean-Philippe Thiran. 2021. Self-Attentive Spatial Adaptive Normalization for Cross-Modality Domain Adaptation. *IEEE Transactions on Medical Imaging* 40 (2021), 2926–2938.

- [82] Nicholas J Tustison, Brian B Avants, Philip A Cook, Yuanjie Zheng, Alexander Egan, Paul A Yushkevich, and James C Gee. 2010. N4ITK: improved N3 bias correction. *IEEE transactions on medical imaging* 29, 6 (2010), 1310–1320.
- [83] Dmitry Ulyanov, Vadim Lebedev, Andrea Vedaldi, and Victor Lempitsky. 2016. Texture networks: Feed-forward synthesis of textures and stylized images. *arXiv preprint arXiv:1603.03417* (2016).
- [84] David C Van Essen, Stephen M Smith, Deanna M Barch, Timothy EJ Behrens, Essa Yacoub, Kamil Ugurbil, Wu-Minn HCP Consortium, et al. 2013. The WU-Minn human connectome project: an overview. *Neuroimage* 80 (2013), 62–79.
- [85] Danyang Wang, Yawen Huang, and Alejandro F Frangi. 2017. Region-Enhanced Joint Dictionary Learning for Cross-Modality Synthesis in Diffusion Tensor Imaging. In *SASHIMI@MICCAI*.
- [86] Jinbao Wang, Guoyang Xie, Yawen Huang, Yefeng Zheng, Yaochu Jin, and Feng Zheng. 2022. FedMed-ATL: Misaligned Unpaired Cross-Modality Neuroimage Synthesis via Affine Transform Loss. *Proceedings of the 30th ACM International Conference on Multimedia* (2022).
- [87] Li Wang, Yaozong Gao, Feng Shi, Gang Li, John H Gilmore, Weili Lin, and Dinggang Shen. 2015. LINKS: Learning-based multi-source Integration framework for Segmentation of infant brain images. *NeuroImage* 108 (2015), 160–172.
- [88] Yan Wang, Luping Zhou, Lei Wang, Biting Yu, Chen Zu, David S. Lalush, Weili Lin, Xi Wu, Jiliu Zhou, and Dinggang Shen. 2018. Locality Adaptive Multi-modality GANs for High-Quality PET Image Synthesis. *Medical image computing and computer-assisted intervention : MICCAI ... International Conference on Medical Image Computing and Computer-Assisted Intervention* 11070 (2018), 329–337.
- [89] Yan Wang, Luping Zhou, Biting Yu, Lei Wang, Chen Zu, David S. Lalush, Weili Lin, Xi Wu, Jiliu Zhou, and Dinggang Shen. 2019. 3D Auto-Context-Based Locality Adaptive Multi-Modality GANs for PET Synthesis. *IEEE Transactions on Medical Imaging* 38 (2019), 1328–1339.
- [90] Zhou Wang and Alan C Bovik. 2002. A universal image quality index. *IEEE signal processing letters* 9, 3 (2002), 81–84.
- [91] Zhou Wang, Alan C Bovik, Hamid R Sheikh, and Eero P Simoncelli. 2004. Image quality assessment: from error visibility to structural similarity. *IEEE transactions on image processing* 13, 4 (2004), 600–612.
- [92] Wen Wei, Emilie Poirion, Benedetta Bodini, Stanley Durrleman, Nicholas Ayache, Bruno Stankoff, and Olivier Colliot. 2018. Learning Myelin Content in Multiple Sclerosis from Multimodal MRI through Adversarial Training. In *MICCAI*.
- [93] Jay West, J Michael Fitzpatrick, Matthew Y Wang, Benoit M Dawant, Calvin R Maurer Jr, Robert M Kessler, Robert J Maciunas, Christian Barillot, Didier Lemoine, Andre Collignon, et al. 1997. Comparison and evaluation of retrospective intermodality brain image registration techniques. *Journal of computer assisted tomography* 21, 4 (1997), 554–568.
- [94] Frank Wilcoxon. 1992. Individual comparisons by ranking methods. In *Breakthroughs in statistics*. Springer, 196–202.
- [95] Guoyang Xie, Jinbao Wang, Yawen Huang, Yuexiang Li, Yefeng Zheng, Feng Zheng, and Yaochu Jin. 2022. FedMed-GAN: Federated Domain Translation on Unsupervised Cross-Modality Brain Image Synthesis.
- [96] Guoyang Xie, Jinbao Wang, Yawen Huang, Yefeng Zheng, Feng Zheng, and Yaochu Jin. 2022. FedMed-ATL: Misaligned Unpaired Brain Image Synthesis via Affine Transform Loss. *ArXiv abs/2201.12589* (2022).
- [97] Bingyu Xin, Yifan Hu, Yefeng Zheng, and Hongen Liao. 2020. Multi-Modality Generative Adversarial Networks with Tumor Consistency Loss for Brain MR Image Synthesis. *2020 IEEE 17th International Symposium on Biomedical Imaging (ISBI)* (2020), 1803–1807.
- [98] Heran Yang, Jian Sun, Aaron Carass, Can Zhao, Junghoon Lee, Jerry L Prince, and Zongben Xu. 2020. Unsupervised MR-to-CT Synthesis Using Structure-Constrained CycleGAN. *IEEE Transactions on Medical Imaging* 39 (2020), 4249–4261.
- [99] Heran Yang, Jian Sun, Liwei Yang, and Zongben Xu. 2021. A Unified Hyper-GAN Model for Unpaired Multi-contrast MR Image Translation. In *MICCAI*.
- [100] Jianchao Yang, John Wright, Thomas S. Huang, and Yi Ma. 2010. Image Super-Resolution Via Sparse Representation. *IEEE Transactions on Image Processing* 19 (2010), 2861–2873.
- [101] Qianye Yang, Nannan Li, Zixu Zhao, Xingyu Fan, EC Chang, Yan Xu, et al. 2018. Mri image-to-image translation for cross-modality image registration and segmentation. *arXiv preprint arXiv:1801.06940* (2018).
- [102] Qianye Yang, Nannan Li, Zixu Zhao, Xingyu Fan, Eric I Chang, Yan Xu, et al. 2020. MRI cross-modality image-to-image translation. *Scientific reports* 10, 1 (2020), 1–18.
- [103] Dong Hye Ye, Darko Zikic, Ben Glocker, Antonio Criminisi, and Ender Konukoglu. 2013. Modality Propagation: Coherent Synthesis of Subject-Specific Scans with Data-Driven Regularization. *Medical image computing and computer-assisted intervention : MICCAI ... International Conference on Medical Image Computing and Computer-Assisted Intervention* 16 Pt 1 (2013), 606–13.
- [104] Xin Yi, Ekta Walia, and Paul S. Babyn. 2019. Generative Adversarial Network in Medical Imaging: A Review. *Medical image analysis* 58 (2019), 101552.
- [105] Biting Yu, Luping Zhou, Lei Wang, Jurgen Fripp, and Pierrick T. Bourgeat. 2018. 3D cGAN based cross-modality MR image synthesis for brain tumor segmentation. *2018 IEEE 15th International Symposium on Biomedical Imaging (ISBI 2018)* (2018), 626–630.
- [106] Biting Yu, Luping Zhou, Lei Wang, Yinghuan Shi, Jurgen Fripp, and Pierrick T. Bourgeat. 2020. Sample-Adaptive GANs: Linking Global and Local Mappings for Cross-Modality MR Image Synthesis. *IEEE Transactions on Medical Imaging* 39 (2020), 2339–2350.
- [107] Ziqi Yu, Yuting Zhai, Xiaoyang Han, Tingying Peng, and Xiao-Yong Zhang. 2021. MouseGAN: GAN-Based Multiple MRI Modalities Synthesis and Segmentation for Mouse Brain Structures. In *MICCAI*.
- [108] Mahmut Yurt, Salman Ul Hassan Dar, Aykut Erdem, Erkut Erdem, and Tolga Çukur. 2021. mustGAN: Multi-Stream Generative Adversarial Networks for MR Image Synthesis. *Medical image analysis* 70 (2021), 101944.

- [109] Matthew D. Zeiler, Dilip Krishnan, Graham W. Taylor, and Rob Fergus. 2010. Deconvolutional networks. *2010 IEEE Computer Society Conference on Computer Vision and Pattern Recognition* (2010), 2528–2535.
- [110] Guodong Zeng and Guoyan Zheng. 2019. Hybrid Generative Adversarial Networks for Deep MR to CT Synthesis Using Unpaired Data. In *MICCAI*.
- [111] Jin Zhang, Xiaohai He, Linbo Qing, Feng Gao, and Bin Wang. 2022. BPGAN: Brain PET synthesis from MRI using generative adversarial network for multi-modal Alzheimer’s disease diagnosis. *Computer Methods and Programs in Biomedicine* 217 (2022), 106676.
- [112] Min Zhang, You Ni, Qinming Zhou, Lu He, Huanyu Meng, Yining Gao, Xinyun Huang, Hongping Meng, Peihan Li, Meilian Chen, Danni Wang, J Hu, Qiu Huang, Yao Li, Fabien Chauveau, Biao Li, and Sheng Chen. 2021. 18F-florbetapir PET/MRI for quantitatively monitoring myelin loss and recovery in patients with multiple sclerosis: A longitudinal study. *EclinicalMedicine* 37 (2021).
- [113] Zizhao Zhang, L. Yang, and Yefeng Zheng. 2018. Translating and Segmenting Multimodal Medical Volumes with Cycle- and Shape-Consistency Generative Adversarial Network. *2018 IEEE/CVF Conference on Computer Vision and Pattern Recognition* (2018), 9242–9251.
- [114] Xingzhong Zhao and Xing-Ming Zhao. 2020. Deep learning of brain magnetic resonance images: A brief review. *Methods* (2020).
- [115] Bo Zhou, Chi Liu, and James S. Duncan. 2021. Anatomy-Constrained Contrastive Learning for Synthetic Segmentation without Ground-truth. In *MICCAI*.
- [116] Bo Zhou, Rui Wang, Ming kai Chen, Adam P. Mecca, Ryan S. O’Dell, Christopher H. van Dyck, Richard E. Carson, James S. Duncan, and Chi Liu. 2021. Synthesizing Multi-Tracer PET Images for Alzheimer’s Disease Patients using a 3D Unified Anatomy-aware Cyclic Adversarial Network. In *MICCAI*.
- [117] Tao Zhou, H. Fu, Geng Chen, Jianbing Shen, and Ling Shao. 2020. Hi-Net: Hybrid-Fusion Network for Multi-Modal MR Image Synthesis. *IEEE Transactions on Medical Imaging* 39 (2020), 2772–2781.
- [118] Jun-Yan Zhu, Taesung Park, Phillip Isola, and Alexei A. Efros. 2017. Unpaired Image-to-Image Translation Using Cycle-Consistent Adversarial Networks. *2017 IEEE International Conference on Computer Vision (ICCV)* (2017), 2242–2251.
- [119] Qing Zuo, Jianping Zhang, and Yin Yang. 2021. DMC-Fusion: Deep Multi-Cascade Fusion With Classifier-Based Feature Synthesis for Medical Multi-Modal Images. *IEEE Journal of Biomedical and Health Informatics* 25 (2021), 3438–3449.